

The Star Formation Rate and Dense Molecular Gas in Galaxies

Yu Gao^{1,2,3} and Philip M. Solomon⁴

1 Purple Mountain Observatory, Chinese Academy of Sciences, 2 West Beijing Road, Nanjing 210008, P.R. China

2 Department of Astronomy, University of Massachusetts,
LGRT B-619E, 710 N. Pleasant St., Amherst, MA 01003

3 Infrared Processing and Analysis Center, California Institute of Technology, MS 100-22, Pasadena, CA 91125

4 Department of Physics & Astronomy, SUNY at Stony Brook, Stony Brook, NY 11794

ABSTRACT

HCN luminosity is a tracer of *dense* molecular gas, $n(H_2) \gtrsim 3 \times 10^4 \text{ cm}^{-3}$, associated with star-forming giant molecular cloud (GMC) cores. We present the results and analysis of our survey of HCN emission from 65 infrared galaxies, including nine ultraluminous infrared galaxies (ULIGs, $L_{\text{IR}} \gtrsim 10^{12} L_{\odot}$), 22 luminous infrared galaxies (LIGs, $10^{11} L_{\odot} < L_{\text{IR}} \lesssim 10^{12} L_{\odot}$), and 34 normal spiral galaxies with lower IR luminosity (most are large spiral galaxies). We have measured the global HCN line luminosity, and the observations are reported in Paper I. This paper analyzes the relationships between the total far-IR luminosity (a tracer of the star formation rate), the global HCN line luminosity (a measure of the total *dense* molecular gas content), and the CO luminosity (a measure of the total molecular content). We find a tight linear correlation between the IR and HCN luminosities L_{IR} and L_{HCN} (in the log-log plot) with a correlation coefficient $R = 0.94$, and an almost constant average ratio $L_{\text{IR}}/L_{\text{HCN}} = 900 L_{\odot}/\text{K km s}^{-1} \text{ pc}^2$. The IR–HCN linear correlation is valid over 3 orders of magnitude including ULIGs, the most luminous objects in the local universe. The direct consequence of the linear IR–HCN correlation is that the star formation law in terms of *dense* molecular gas content has a power law index of 1.0. The global star formation rate is linearly proportional to the mass of dense molecular gas in normal spiral galaxies, LIGs, and ULIGs. This is strong evidence in favor of star formation as the power source in ultraluminous galaxies since the star formation in these galaxies appears to be normal and expected given their high mass of dense star-forming molecular gas.

The HCN–CO correlation is also much tighter than the IR–CO correlation. We suggest that the nonlinear correlation between L_{IR} and L_{CO} may be a consequence of the stronger and perhaps more physical correlations between L_{IR} and L_{HCN} and between L_{HCN} and L_{CO} . Thus, the star formation rate indicated by L_{IR} depends on the amount of dense molecular gas traced by HCN emission, not the total molecular gas traced by CO emission. One of the main arguments in favor of an active galactic nucleus (AGN) as the power source in ULIGs is the anomalously high ratio $L_{\text{IR}}/L_{\text{CO}}$ or $L_{\text{IR}}/\text{M(H}_2\text{)}$ or high star formation rate per M_{\odot} of gas, compared with that from normal spiral galaxies. This has been interpreted as indicating that a dust-enshrouded AGN is required to produce the very high luminosity. Viewed in terms of the dense gas mass the situation is completely different. The ratio $L_{\text{IR}}/L_{\text{HCN}}$ or $L_{\text{IR}}/\text{M}_{\text{dense}}$, a measure of the star formation rate per solar mass of *dense* gas is essentially the same in all galaxies including ULIGs. The ratio $L_{\text{IR}}/\text{M}_{\text{dense}}$ is virtually independent of galaxy luminosity and on average $L_{\text{IR}}/\text{M}_{\text{dense}} \approx 90 L_{\odot}/M_{\odot}$, about the same as in GMC cores but much higher than in GMCs. We find that ULIGs simply have a large quantity of dense molecular gas and thus produce a prodigious starburst that heats the dust, produces the IR, and blocks all or most

optical radiation. The HCN global luminosity may be used as an indicator of the star formation rate in high-redshift objects including hyperluminous galaxies.

The HCN/CO ratio is an indicator of the dense molecular gas fraction. and gauges the globally averaged molecular gas density. We find that the HCN/CO ratio is a powerful starburst indicator. All galaxies in our sample with a high dense gas mass fraction indicated by $L_{\text{HCN}}/L_{\text{CO}} > 0.06$ are LIGs or ULIGs. Normal spirals all have similar and low dense gas fractions $L_{\text{HCN}}/L_{\text{CO}} = 0.02$ to 0.05 . The global star formation efficiency depends on the fraction of the molecular gas in a dense phase.

Subject headings: galaxies: ISM — galaxies: starburst — infrared: galaxies — ISM: molecules — radio lines: galaxies

1. INTRODUCTION

Stars are born in the molecular interstellar medium, the raw material for star formation. In the Milky Way, all star formation essentially takes place in molecular clouds and most star formation takes place in giant molecular clouds (GMCs; Solomon, Sanders, & Scoville 1979) with mass $M > 10^5 M_{\odot}$ and not the diffuse neutral ISM dominated by atomic hydrogen (extended HI gas disk). The star formation rate (SFR) of molecular clouds can be estimated from the far-infrared (FIR) luminosity emitted by the warm dust heated by embedded high-mass OB stars (e.g., Mooney & Solomon 1988). The mass of molecular gas can be determined from the CO luminosity calibrated by γ ray flux from the interaction of cosmic rays with hydrogen molecules (e.g., Bloemen et al. 1986) or by dynamical cloud masses determined from CO kinematics for virialized individual molecular clouds (Solomon et al. 1987; Young & Scoville 1991). These methods are in good agreement (see Solomon & Barrett 1991). All strong high-mass star formation regions are associated with GMCs, especially the cores of GMCs. The ratio of FIR luminosity to the CO luminosity, or to the cloud mass, a measure of the SFR per solar mass of the cloud and an indicator of star formation efficiency (SFE), ranges over a factor of 100 for different clouds, and over a factor of 1000 from clouds to the cores of GMCs (e.g., Mooney & Solomon 1988; Plume et al. 1997). An understanding of the physical conditions in GMCs and their relation to galactic dynamics is a prerequisite to the understanding of the star formation process, the SFR in galaxies and starbursts.

Star formation in galaxies is closely tied up with the local gas density, as formulated in the Schmidt (1959) law, although the important component is the molecular gas. Globally, the SFR correlates with the molecular gas content in galaxies, as traced by CO emission, including luminous and ultraluminous infrared galaxies (LIGs and ULIGs¹). In Galactic star-forming regions, active high-mass star formation is intimately related to the very dense molecular gas in the cores. While the canonical molecular gas tracer CO shows strong emission in cloud cores, it is not specific enough to reveal their star formation potential. The bulk of the cloud material traced by CO observations is in the GMC envelopes and is at a much lower density. The physical conditions of active star-forming GMC cores are better revealed by emission from very high transition CO lines (in the submillimeter regime) and high dipole-moment molecules like CS and HCN.

¹LIGs: $10^{12} L_{\odot} \gtrsim L_{\text{IR}} > 10^{11} L_{\odot}$, ULIGs: $L_{\text{IR}} \gtrsim 10^{12} L_{\odot}$ (to be exact, $10^{11.9} L_{\odot}$ in this paper). For a definition of the total IR (8 to $1000 \mu\text{m}$) luminosity L_{IR} and FIR luminosity L_{FIR} , see Sanders & Mirabel (1996). The value of L_{IR} is generally larger, by up to $\sim 20\%$ as it includes both 12 and $25 \mu\text{m}$ emission, than L_{FIR} . However, we often simply refer the total IR emission as FIR in this paper.

HCN is one of the most abundant high dipole-moment molecules that traces molecular gas at densities $n(H_2) \gtrsim 3 \times 10^4 \text{ cm}^{-3}$, more than 2 orders of magnitude higher than that traced by CO ($\gtrsim 300 \text{ cm}^{-3}$). Many HCN (1-0) observations have already been conducted by different groups (Nguyen-Q-Rieu et al. 1989, 1992; Henkel et al. 1990; Solomon, Downes, & Radford 1992; Israel 1992; Helfer & Blitz 1993; Aalto et al. 1995; Curran, Aalto, & Booth 2000) in a variety of nearby galaxies. These previous observations contain small samples with frequent overlap in the sample selection. The total number of galaxies detected in HCN is still small ($\lesssim 30$), and for many galaxies only the central position was observed. Gao & Solomon (2003, hereafter Paper I), in the companion paper, have presented a systematic survey of global HCN luminosity that more than doubles the number of galaxies (~ 60) observed in HCN.

Although the dense molecular gas is strongly concentrated in the central regions ($\lesssim 1 \text{ kpc}$), HCN mapping of a dozen nearby galaxies out to a diameter of $\sim D_{25}/4$ (Gao 1996, 1997; Y. Gao & P.M. Solomon 2004, in preparation) shows that a substantial fraction of HCN emission originates from the inner disks outside the central $\sim 1 \text{ kpc}$. All previous HCN observations in external galaxies including a few HCN maps (e.g., Nguyen-Q-Rieu et al. 1992; Reynaud & Downes 1997; Helfer & Blitz 1997a) have primarily been observations of the galactic central regions. In most cases, the total HCN emission from the entire galaxy has not been measured. The recent HCN observations in 20 Seyfert galaxies are primarily of the galaxy centers, and many are nondetections or marginal detections (Curran et al. 2000). Confusion may occur when the results drawn from the HCN observations of central regions of galaxies are compared with the global properties of galaxies. Aalto et al. (1995) have not found a correlation between the molecular line intensity ratio, $I_{\text{CO}}/I_{\text{HCN}}$, and FIR emission, or measures of star-forming activity in their sample of 10 interacting galaxies, which appeared to be in conflict with the original findings of a tight FIR-HCN correlation in another sample of 10 LIGs/ULIGs and spiral galaxies where the total HCN emission was measured (Solomon et al. 1992). The situation has now been clarified by our new HCN survey of ~ 60 galaxies (Paper I), which measured the global HCN emission in a wide range of galaxies. There is indeed a tight FIR-HCN correlation in a statistically significant HCN sample.

It is clear from all previous observations that the molecular gas in the central regions of spiral galaxies, starbursts, and LIGs/ULIGs is much denser than the molecular ISM in the disks of spiral galaxies (e.g., Nguyen-Q-Rieu et al. 1992; Solomon et al. 1992; Helfer & Blitz 1997a; Wild & Eckart 2000). From various observational studies of star-forming regions of GMCs in the Milky Way, it is also clearly shown that the active star-forming regions in the disk are the dense molecular cloud cores (e.g., Mooney & Solomon 1988; Plume et al. 1997; Pirogov 1999; Evans 1999) rather than the entire molecular envelopes of GMCs. The SFE of active star-forming clouds that are associated with IR sources readily apparent on *IRAS* 60 and 100 μm images can be 100 times higher than the IR-quiet clouds with no apparent IR sources revealed by *IRAS* (Mooney & Solomon 1988). Star formation efficiency ($L_{\text{IR}}/L_{\text{CO}}$) can vary over a factor of 100 as well in galaxies.

Normal spiral galaxies have an SFE similar to that of Galactic GMCs, whereas the SFE of ULIGs/LIGs and advanced mergers can be more than an order of magnitude larger (e.g., Solomon & Sage 1988; Solomon et al. 1997; Gao & Solomon 1999). These differences in SFE can be understood in terms of the different dense molecular gas content as traced by HCN observations.

For 10 galaxies, including both LIGs/ULIGs and normal spiral galaxies, Solomon et al. (1992) show that there is a tight correlation between the ratio of the IR and CO luminosities $L_{\text{IR}}/L_{\text{CO}}$ and the HCN/CO luminosity ratio $L_{\text{HCN}}/L_{\text{CO}}$ in addition to the excellent correlation between L_{IR} and L_{HCN} . This is now fully confirmed with our current HCN study of a sample of 65 galaxies (§3). These correlations demonstrate a close relationship between the SFR and the *dense molecular gas reservoir* in galaxies. The SFE depends

on the fraction of available molecular gas in a dense phase ($L_{\text{HCN}}/L_{\text{CO}}$), and the dense molecular content of even gas-rich spirals is much less than that of LIGs/ULIGs of comparable total molecular gas content (Solomon et al. 1992; Radford 1994). Since CO emission traces most of the molecular gas mass and is not necessarily a specific tracer of the *dense* molecular gas (e.g., Mauersberger & Henkel 1993; Evans 1999) or the IR luminosity from star formation (Mooney & Solomon 1988), CO alone can give a misleading picture of the densest molecular gas in a galaxy.

In Galactic plane GMCs, for example, essentially all OB star formation occurs in the cores of GMCs with strong CS and HCN emission. The ratios of CO/CS and CO/HCN intensities for Galactic disk GMCs are much larger than for Galactic center clouds (Lee, Snell, & Dickman 1990; Jackson et al. 1996; Plume et al. 1997; Helfer & Blitz 1997b) and an order of magnitude larger than for the archetypal ULIG Arp 220 (Solomon, Radford, & Downes 1990). In some galaxies, the molecular gas in the center is much more prominent in HCN emission than in CO. A good example is the center of the Seyfert 2/starburst hybrid galaxy NGC 1068, where all interferometric maps demonstrate that the nuclear region is more prominent than the rings or spiral arms when viewed in HCN, while the opposite is true in CO emission (Tacconi et al. 1997, 1994; Helfer & Blitz 1995; Jackson et al. 1993). A similar trend is also observed in the centers of M51 and NGC 1097 (e.g., Kohno et al. 1996, 2003).

Here we utilize a large, statistically significant sample with observations of global HCN emission from 65 spiral galaxies, LIGs, and ULIGs — 53 from the systematic HCN survey of Paper I, 10 from Solomon, Downes, & Radford (1992), plus two from the literature. These galaxies range over 3 orders of magnitude in FIR luminosity. We analyze the various relationships among the global HCN, CO, and FIR luminosities. We further discuss the physical relationship between the dense molecular gas content and the rate of high-mass star formation in galaxies.

The HCN sample and observations are briefly reviewed in §2. Section 3 presents the results. Section 3.1 is a comparison of the IR–HCN and IR–CO correlations. Section 3.2 concentrates on the importance of the dense gas mass fraction and the star formation efficiency. Section 3.3 and the Appendices present multi-parameter fits to the data and the effect of dust temperature. Section 3.4 has a brief summary of all results. In §§4.1–4.3, we discuss the importance of HCN as a tracer of star-forming molecular gas, the star formation rate as a function of the dense gas mass, and the global star formation law. Section 4.4 discusses the HCN/CO ratio as a starburst indicator. Section 4.5 discusses the origin of FIR emission from spirals and ULIGs. Section 4.6 briefly speculates on the implications for hyperluminous infrared galaxies at high z . Finally, we summarize the main points of our study in §5.

2. THE HCN SURVEY

The detailed descriptions of our survey sample and HCN (and CO) observations were given in the companion paper (Paper I). Our HCN survey sample is drawn from samples in recent CO observations of galaxies showing strong CO emission (e.g., the CO antenna brightness temperature much larger than 100 mK for normal spiral galaxies and larger than 20 mK for LIGs/ULIGs). All truly IR-bright galaxies with 60 or 100 μm emission larger than 50 or 100 Jy, respectively, have also been included. Essentially all galaxies with strong CO and IR emission in northern sky have been chosen for the HCN survey.

We carried out several observing runs mainly with the former NRAO² 12m telescope at Kitt Peak,

²The National Radio Astronomy Observatory is operated by Associated Universities, Inc., under cooperative agreement with

the IRAM 30m telescope at Pico Veleta near Granada, Spain, and the FCRAO 14m telescope for most of our observations. We here only mention our observing strategy of using different telescopes. The IRAM 30m was mostly used to observe ULIGs (rather distant) and to map out some nearby starburst galaxies of smaller optical diameters, given the small matching beam size as compared with the source extent for effective mapping. Essentially all other observations were conducted with the NRAO 12m so that one beam measurement can cover almost all HCN emission from relatively distant galaxies, including some merging galaxy pairs. Also almost all nearby large spiral galaxies have been at least mapped along the major axes with the NRAO 12m, and only a few of them were initially tried mapping with the QUARRY receivers at the FCRAO 14m (because of its limited sensitivity).

The goal of the HCN survey of Paper I is to determine the total HCN emission from the whole inner disks or the entire galaxies in a large sample of galaxies with a wide range of IR luminosity. Combined with the HCN data of 12 galaxies, 10 from Solomon et al. (1992), including a half-dozen LIGs/ULIGs, and the other two galaxies, M51 (Nguyen-Q-Rieu et al. 1992) and NGC 4945 (Henkel, Whiteoak, & Mauersberger 1994) that were mapped extensively in HCN, we have a large, statistically significant sample of 65 galaxies with globally measured HCN emission. In addition, there are more than a dozen nearby large spiral galaxies with HCN detections toward the galactic nuclei (Nguyen-Q-Rieu et al. 1992; Helfer & Blitz 1993; Aalto et al. 1995; Curran et al. 2000), including LIGs (e.g., NGC 3256, Casoli, Dupraz & Combes 1992) that do not overlap with our HCN survey sample³. In principle, we could further enlarge our HCN sample to a total of about 80 galaxies. These observations of nearby galaxies did not measure the total HCN emission, however, with only the central/nuclear HCN emission observed. Therefore, most HCN data in these nearby galaxies can thus only be used to set lower limits to the total HCN luminosities. Further HCN observations at least along the major axes are required to map out the total HCN emission. For the sake of completeness, consistency, and uniformity of our sample, these galaxies with lower HCN limits in the literature are not included in our sample.

The derived global properties of the line luminosities and various luminosity ratios of galaxies in the HCN survey sample are listed in Table 1 (cf. Table 4 in Paper I), together with a dozen galaxies where the total HCN luminosities are available or can be estimated from the literature. There are also several other fairly distant galaxies in Curran et al. (2000) and Aalto et al. (1995) in which the global HCN luminosities were supposedly measured, but we did not include them in our sample as their data seem to have low signal-to-noise ratio. Mrk 273, one of the galaxies that overlaps in both of our sample and that of Curran et al. (2000), for example, was claimed to be detected with an extremely large HCN/CO luminosity ratio of 1. Our high-quality IRAM 30m spectra (Paper I), however, clearly indicate an HCN/CO intensity ratio of $\sim 1/6$ and a HCN/CO luminosity ratio of 0.23, which is consistent with all other ULIGs that have been significantly detected in HCN so far, rather than an unrealistic ratio of ~ 1 .

We also have some limits to the total HCN line emission owing to insufficient mapping of HCN (about 10 % of the galaxies in our sample), but our HCN lower limits are probably close to the true values as we have some off-nucleus HCN measurements besides the central beams on the nuclei in most cases. We keep these sensitive HCN limits in Table 1 and include these data for the various analyses.

the National Science Foundation.

³However, Curran et al. (2001) submitted and published several HCN maps (though mostly still very limited spatial coverage of only central 1'–2' regions) of nearby Seyfert galaxies after we submitted our paper.

3. RESULTS AND ANALYSIS

3.1. Comparison of the IR–HCN and IR–CO Correlations

The principal observational result from this survey is the tight linear relation observed between far-infrared luminosity, L_{IR} , and HCN line luminosity, L_{HCN} , shown in Figure 1a. This very good correlation extends over 3 orders of magnitude in luminosity and includes normal spiral galaxies and luminous and ultraluminous infrared galaxies (LIGs/ULIGs). Figure 1b shows the correlation between L_{IR} and L_{CO} of the same sample, which has a larger scatter than the FIR–HCN relation and most importantly steepens with higher IR luminosity, showing the well-known result that LIGs/ULIGs, although rich in molecular gas, have a substantially higher IR luminosity per unit CO luminosity or per solar mass of molecular gas H_2 (e.g., Solomon et al. 1997).

A least-squares fit using all the data but excluding HCN limits yields a power-law slope of 1.00 ± 0.05 and 1.25 ± 0.08 for $L_{\text{IR}}-L_{\text{HCN}}$ and $L_{\text{IR}}-L_{\text{CO}}$, respectively. The corresponding correlation coefficients (squared) are $R^2 = 0.88$ and 0.77 . The slopes change to 1.05 ± 0.05 and 1.44 ± 0.08 for $L_{\text{IR}}-L_{\text{HCN}}$ and $L_{\text{IR}}-L_{\text{CO}}$, respectively, if an orthogonal fit is used. Including the sources with HCN limits in the fit has little effect on the slope or the fit. The best-fit (logarithmic) relation between HCN and IR luminosities excluding galaxies with upper or lower limits is

$$\log L_{\text{IR}} = 1.00(\pm 0.05) \log L_{\text{HCN}} + 2.9, \text{ or } L_{\text{IR}}/L_{\text{HCN}} = 900 L_{\odot}/\text{K km s}^{-1} \text{ pc}^2, \quad (1)$$

indeed a linear relation. When we use all galaxies including HCN limits the correlation remains almost the same with $\log L_{\text{IR}} = 0.97 \log L_{\text{HCN}} + 3.1$ and with the same correlation coefficient ($R=0.94$).

At first glance of Figure 1, the correlation between L_{CO} and L_{IR} may appear to be nearly as good as that of the $L_{\text{HCN}}-L_{\text{IR}}$ correlation, even though there is significant difference in the correlation coefficients and the dispersion from the fit. The most obvious difference occurs at the high L_{IR} end. In Figure 1b, a line of constant $L_{\text{IR}}/L_{\text{CO}} = 33 L_{\odot}/\text{K km s}^{-1} \text{ pc}^2$ fits the lower luminosity galaxies but lies well below almost all (28/31) of the high-luminosity galaxies (LIGs/ULIGs). The correlation between L_{IR} and L_{HCN} still fits the ratio determined from lower IR luminosities ($L_{\text{IR}} < 10^{11} L_{\odot}$), but the correlation between L_{CO} and L_{IR} does not. (The lines shown in Fig. 1 are the fits of a fixed slope of 1 to low-luminosity galaxies.) The FIR–HCN relation is linear all the way up to $L_{\text{IR}} = 10^{12.5} L_{\odot}$, but the FIR/CO ratio is systematically higher for high-luminosity galaxies than for those of normal luminosity.

One obvious difference between the FIR–CO and FIR–HCN relationships is that the range of CO luminosity is only 2 orders of magnitude, whereas HCN luminosity covers 3 orders of magnitude, almost the same as the IR luminosity. For LIGs/ULIGs the CO is systematically weak compared with the IR. Measurements of CO luminosity of a large sample of ULIGs (Solomon et al. 1997; most of which are not in Fig. 1b since there are no corresponding HCN observations available) show that they all lie above the fitted line in Figure 1b.

Another way to demonstrate these points is to compare the luminosity ratios of $L_{\text{IR}}/L_{\text{HCN}}$ and $L_{\text{IR}}/L_{\text{CO}}$ with L_{IR} (Fig. 2). $L_{\text{IR}}/L_{\text{HCN}}$ appears to be nearly independent of L_{IR} , whereas the $L_{\text{IR}}/L_{\text{CO}}$ ratio increases substantially with increasing L_{IR} as established by previous work (e.g., Young et al. 1989; Sanders, Scoville, & Soifer 1991). These results are also revealed in Table 2, which summarizes the average IR, CO, and HCN luminosities among ULIGs, LIGs, normal spiral galaxies, and all galaxies of the entire HCN sample.

In summary, the IR–HCN correlation is linear and is extremely tight over 3 orders of magnitude

in luminosity, when compared with the nonlinear IR–CO correlation. While the high luminosity of LIGs/ULIGs requires an elevated SFE of the total molecular gas indicated by $L_{\text{IR}}/L_{\text{CO}}$, the SFR per unit of *dense* molecular gas—the SFE of the *dense* molecular gas indicated by $(L_{\text{IR}}/L_{\text{HCN}})$ —is almost constant and independent of the IR luminosity or total SFR. The tight relationship between L_{IR} and L_{HCN} will be further illustrated by comparing it with other correlations in the following two sections (§3.2 & §3.3).

3.2. Dense Molecular Gas Fraction ($L_{\text{HCN}}/L_{\text{CO}}$) and Star Formation Efficiency ($L_{\text{IR}}/L_{\text{CO}}$)

Figure 3 shows a significant correlation between HCN and CO luminosities with a correlation coefficient $R=0.92$ ($R^2 = 0.85$). In all figures, except where L_{IR} is itself explicitly plotted, we distinguish LIGs/ULIGs ($L_{\text{IR}} > 10^{11} L_{\odot}$, filled circles) from the less luminous normal spiral galaxies (open circles) so that any systematic difference between these two subsamples can easily be seen. This suggests that the more gas-rich galaxies tend to have more dense molecular gas (and vice versa), and thus are more luminous (Fig. 1). The correlation is much better for normal galaxies (open circles) than for LIGs/ULIGs (filled circles). For normal spiral galaxies there is a tight relationship between the HCN and CO luminosities with a slope of 1.0, shown as the fit line in Figure 3. There is also a very small dispersion about the fit with $\sigma(\log L_{\text{HCN}}) = 0.14$. This good linear HCN–CO correlation is the underlying reason that the FIR–CO correlation is linear for normal galaxies and CO luminosity is reasonably good at predicting their SFR (FIR).

All but three of the 31 LIGs have L_{HCN} above the linear fit (Fig. 3) determined from normal spirals, clearly showing that excess HCN emission compared with CO emission is a characteristic of LIGs/ULIGs. An orthogonal fit to all galaxies gives a nonlinear relation:

$$\log L_{\text{HCN}} = 1.38 \log L_{\text{CO}} - 4.79, \text{ or } \frac{L_{\text{HCN}}}{L_{\text{CO}}} = 0.1 \left(\frac{L_{\text{CO}}}{10^{10} \text{Kkm s}^{-1} \text{pc}^2} \right)^{0.38}. \quad (2)$$

It is the high ratio of HCN/CO for LIGs/ULIGs that causes the breakdown in the IR–CO relation.

A high ratio of $L_{\text{HCN}}/L_{\text{CO}}$ is a distinguishing feature of LIGs/ULIGs. As can be seen from Table 2, the average ratio systematically increases as IR luminosity increases. Figure 4 shows the IR luminosity of all 65 galaxies in the sample as a function of the ratio $L_{\text{HCN}}/L_{\text{CO}}$. It is immediately apparent that LIGs/ULIGs ($L_{\text{IR}} > 10^{11} L_{\odot}$) have systematically higher HCN/CO ratios than normal galaxies. However, for normal spirals only, although there is some scatter with $L_{\text{HCN}}/L_{\text{CO}} = 0.02\text{--}0.06$, there is no correlation between IR and $L_{\text{HCN}}/L_{\text{CO}}$. All of the most luminous galaxies, i.e., ULIGs, have high $L_{\text{HCN}}/L_{\text{CO}} > 0.09$. The most striking result is that *all* (27/27) galaxies with $L_{\text{HCN}}/L_{\text{CO}} > 0.06$ are luminous (or ultraluminous). The 2 most luminous galaxies in our sample Mrk 231 and IRAS 17208-0014 have HCN/CO = 0.23 and 0.25, respectively. The molecular ratio $L_{\text{HCN}}/L_{\text{CO}}$ appears to be 100% successful as an indicator of galaxies with infrared starbursts. In § 4 we further discuss the contributions of the disk and nuclear regions to these global values of L_{HCN} and L_{CO} as well as the $L_{\text{HCN}}/L_{\text{CO}}$ ratio.

While all galaxies with a high HCN/CO ratio are IR-luminous, it is not true that all LIGs have a high dense gas fraction, $L_{\text{HCN}}/L_{\text{CO}}$. There are a group of seven LIGs in our sample that are IR luminous and have high HCN luminosities but normal ratios of HCN/CO. These are gas-rich (CO-luminous) galaxies with normal SFE. They are the filled circles on the normal galaxy fit line in Figure 3 and in the upper left of Figure 4. Their high L_{IR} is simply the result of a tremendous amount of available molecular gas and a normal fraction of dense molecular gas. In this sense they are not starbursts globally. They are globally using their molecular gas at a normal SFR. Some of the notable examples in our sample are Mrk 1027, NGC 1144 (Gao et al. 1997), NGC 6701, and even Arp 55 (Table 1). Luminous prestarburst galaxies like

Arp 302 (Gao 1996; Lo, Gao, & Gruendl 1997), and even early stage galaxy mergers in the initial starburst phase with extended CO emission (e.g., NGC 6670, Wang et al. 2001), belong to this category as well.

Figure 5a shows a correlation between $L_{\text{IR}}/L_{\text{CO}}$ and $L_{\text{HCN}}/L_{\text{CO}}$ with a correlation coefficient $R = 0.74$ ($R^2 = 0.55$, there is little effect on the fit whether those HCN limits are used or not). This suggests that the star formation efficiency, SFE ($L_{\text{IR}}/L_{\text{CO}}$), depends on the fraction of molecular gas in a dense phase indicated by $(L_{\text{HCN}}/L_{\text{CO}})$. This correlation demonstrates the direct connection between the IR and HCN luminosities (as shown in Fig. 1a). Both L_{IR} and L_{HCN} have been normalized by L_{CO} to show the physical relationship between L_{IR} and L_{HCN} after removing the dependence upon distance, galaxy size, and other possible selection effects. Of course, the range of the ratio $(L_{\text{HCN}}/L_{\text{CO}})$ is less than that for L_{HCN} and the correlation is not as strong as in Figure 1a, although the dispersion about the fit is almost the same. This normalization is dust extinction-free, unlike the use of, for example, the blue luminosity in the normalization.

Similarly, we can show the correlation between L_{IR} and L_{CO} divided by L_{HCN} for normalization. Surprisingly, the strong correlation observed in Figure 1b has completely disappeared, and there is no correlation left at all ($R^2 = 0.01$; Fig. 5b). This certainly reflects the tight correlation between IR and HCN and the fact that $L_{\text{IR}}/L_{\text{HCN}}$ is almost independent of galaxy luminosity (Fig. 2a). The absence of a correlation in Figure 5b also implies that the apparent well-known correlation between L_{IR} and L_{CO} may lack a true physical basis, at least as compared with that between L_{IR} and L_{HCN} . The IR–CO correlation may be due to a combination of the tighter IR–HCN and HCN–CO correlations. Nevertheless, $L_{\text{IR}}/L_{\text{HCN}}$ is not completely independent of the CO luminosity (see §3.3 and the appendix) as its inverse $L_{\text{HCN}}/L_{\text{IR}}$ is weakly correlated with $L_{\text{CO}}/L_{\text{IR}}$ with a correlation coefficient $R = 0.56$ ($R^2 = 0.31$, still a meaningful correlation as a consequence of the tight HCN–CO correlation normalized by L_{IR}).

3.3. The Model Parameter Fits

Table 3 in Appendix B summarizes almost all the parameter fits in the IR, CO, and HCN data sets including the warm dust temperature deduced from the 60 and 100 μm fluxes. Here we discuss the three-parameter fits involving the IR, HCN, and CO luminosities and the warm dust temperature T_{dust} dependence of the luminosity ratios. Further details of various other correlation fits are also discussed in the Appendix. These fits to the data demonstrate that the two important independent parameters are the IR and HCN luminosities.

3.3.1. Multi-parameter Fits

The IR luminosity from a model fit to the HCN and CO [the $\text{IR}(L_{\text{HCN}}, L_{\text{CO}})$ model] yields

$$\log L_{\text{IR}}(L_{\text{HCN}}, L_{\text{CO}}) = 2.28 + 0.88 \log L_{\text{HCN}} + 0.16 \log L_{\text{CO}}. \quad (3)$$

The weak dependence on L_{CO} shows that the IR luminosity is determined principally from the HCN luminosity. The dispersion about the fit is almost the same as the two parameter fit of $L_{\text{IR}}-L_{\text{HCN}}$. The ratio for L_{CO} (0.98) is very small as compared with that for L_{HCN} (6.95), demonstrating that L_{CO} is almost random after fitting L_{HCN} for L_{IR} .

An IR and CO luminosity model fit for L_{HCN} [the $\text{HCN}(L_{\text{IR}}, L_{\text{CO}})$ model] gives

$$\log L_{\text{HCN}}(L_{\text{IR}}, L_{\text{CO}}) = -2.62 + 0.56 \log L_{\text{IR}} + 0.49 \log L_{\text{CO}}. \quad (4)$$

Here, L_{IR} and L_{CO} seem to be almost equally important. This relation produces a tighter fit than either of the two-parameter fits HCN-CO (Fig. 3) or HCN-IR (Fig. 1a).

Therefore, although the HCN luminosity depends on both the CO and IR luminosity, the IR is predicted almost entirely by the HCN with almost no effect from the CO luminosity. The reason for this surprising result is probably that, of the three separate two-parameter (IR-HCN, HCN-CO, and IR-CO) fits, the weakest and the one that has the largest dispersion of the data from the fit is the IR-CO correlation.

The corresponding fit for the CO luminosity is

$$\log L_{\text{CO}}(L_{\text{IR}}, L_{\text{HCN}}) = 3.60 + 0.55 \log L_{\text{HCN}} + 0.12 \log L_{\text{IR}}. \quad (5)$$

It is clear that the CO is more closely related to the HCN than to the IR luminosity. In other words, the dependence of the CO luminosity on the IR is much weaker than on the HCN luminosity. This result is probably due to the very tight correlation between CO and HCN for normal galaxies (Fig. 3).

3.3.2. Warm Dust Temperature Dependence

Here we examine the influence of the warm dust temperature on the luminosity ratios. It is well known that the warm dust temperature is an important parameter in the IR-CO correlation (e.g., Young et al. 1986; Young & Scoville 1991). Calculating the warm dust temperature from the 60/100 μm flux ratio, we find that the $L_{\text{IR}}/L_{\text{CO}}$ luminosity ratio depends strongly on T_{dust} (see figures in the appendix)

$$L_{\text{IR}}/L_{\text{CO}} = 61(T_{\text{dust}}/35\text{K})^{5.7}, \quad (6)$$

for optically thin dust with emissivity $\sim \nu^\beta$ ($\beta = 1.5$).

As we can see from Figure 2a, the ratio $L_{\text{IR}}/L_{\text{HCN}}$ is almost independent of IR luminosity. If we fit this ratio to the dust temperature (poor correlation), we find a weak correlation with

$$L_{\text{IR}}/L_{\text{HCN}} \sim 980(T_{\text{dust}}/35\text{K})^{1.8}. \quad (7)$$

The IR-HCN relation changes only by a factor of 2 on average across the entire temperature range of the sample galaxies ($T = 29$ to 46K), while the IR-CO ratio changes by a factor of 13. The HCN/CO ratio changes with the dust temperature between these two extremes since (using eqs. [6] and [7])

$$L_{\text{HCN}}/L_{\text{CO}} = (L_{\text{IR}}/L_{\text{CO}})/(L_{\text{IR}}/L_{\text{HCN}}) \sim T_{\text{dust}}^{3.9}. \quad (8)$$

Indeed, a direct fit to the data (still a reasonable correlation with $R^2 \sim 0.5$) gives $L_{\text{HCN}}/L_{\text{CO}} \sim T_{\text{dust}}^{3.6}$.

3.4. Summary of the Results

Our results presented in Figures 1–5 show that dense molecular gas mass indicated by HCN luminosity is a much better predictor of infrared luminosity and star formation than total H_2 content indicated by CO

luminosity. We identify two types of LIGs according to their total molecular gas content. Both types have high total L_{HCN} in addition to high L_{IR} . Most LIGs have a high dense molecular gas fraction, but a second group has a normal ratio of HCN/CO yet a very high CO luminosity. Are both types of LIGs starbursts? It may well be that LIGs with a normal $L_{\text{HCN}}/L_{\text{CO}}$ are not necessarily genuine starbursts since the infrared luminosity can be produced by a large amount of molecular gas forming stars at a normal rate (efficiency). Star formation efficiency can remain almost unchanged, whether galaxies are molecular gas-rich (more luminous) or relatively gas-poor (less luminous, cf. Young 1999). However, SFE increases dramatically from *dense* molecular gas-poor galaxies to *dense* molecular gas-rich galaxies. All galaxies with a dense gas mass fraction $L_{\text{HCN}}/L_{\text{CO}} > 0.06$ are LIGs or ULIGs in our sample. In essence, HCN traces the molecular gas at high density and at high warm dust temperature that is tightly linked to the active star formation.

4. DISCUSSION

4.1. HCN — Tracer of Active Star-forming Dense Molecular Gas

All the parameter fits essentially show the same thing. CO luminosity by itself leads to a rough prediction for IR luminosity that breaks down for luminous infrared galaxies (LIGs), especially for ultraluminous infrared galaxies (ULIGs), whereas HCN luminosity is much better at predicting the IR luminosity for all galaxies including ULIGs. Therefore, the star formation rate (SFR) indicated by L_{IR} in galaxies depends on the amount of dense molecular gas traced by HCN, not the total molecular gas content measured by CO. In particular, the IR–CO correlation may not have a solid physical basis as it can be readily related to the stronger and perhaps more physical IR–HCN and HCN–CO correlations, which may be the origin of the correlation between IR and CO. This is reminiscent of the poor IR–HI correlation as compared with the better IR–CO correlation that became apparent two decades ago, when systematic CO observations of significant numbers of galaxies became available.

The HCN radiation is associated with the warm dust traced by the FIR radiation, whereas the total molecular gas traced by CO originates in diverse dust components at different temperatures. The temperature dependence of L_{IR} (or $L_{60\mu\text{m}}$ or $L_{100\mu\text{m}}$) is straight-forward to understand since it is just the Planck law plus the dust emissivity. In this perspective, it is easy to see why the $L_{\text{IR}}-L_{\text{CO}}$ relation has a strong dependence upon the dust temperature term since L_{CO} at most is proportional to the first power of the temperature, while L_{IR} (or $L_{100\mu\text{m}}$), depending on the emissivity law, is proportional to at least the fifth power of the dust temperature. Therefore, many correlations that involve T_{dust} and L_{CO} [see Appendix, e.g., in one case as represented in the $\text{CO}(L_{100\mu\text{m}}, T_{\text{dust}})$ model, $\log L_{\text{CO}} = 5.07 + 0.88 \log L_{100\mu\text{m}} - 3.0 \log T_{\text{dust}}$] can be easily explained. The more complex question is why this T_{dust} dependence almost entirely goes away for the L_{HCN} , e.g., the $\text{HCN}(L_{100\mu\text{m}}, T_{\text{dust}})$ model, $\log L_{\text{HCN}} = -1.12 + 0.95 \log L_{100\mu\text{m}} - 0.2 \log T_{\text{dust}}$, and similarly others involving L_{HCN} (Table 3). The simple answer to this is that the higher molecular gas density produces more active star formation, which raises T_{dust} owing to heating of the newborn stars. High molecular gas density, strong HCN emission, and warm dust temperature go together. HCN traces the active star-forming molecular gas where both the molecular gas density and dust temperature are high.

We have already shown in Paper I that HCN emission in galaxies is primarily due to the collisional excitation by high-density molecular hydrogen, not radiative excitation through the mid-IR pumping (see also Stutzki et al. 1988; Paglione et al. 1997). Even though the mid-IR pumping is not a significant source to excite the rotational transition of HCN emission, there are still some other possibilities that may help excite HCN, e.g., collisions with electrons (Aalto et al. 1995), the possibly enhanced HCN abundance and

shock excitation, owing to excess supernovae occurred in starburst galaxies and LIGs/ULIGs. However, all these, even collectively, are only a secondary effect on a global scale in galaxies, although significant contribution in a particularly favorable environment in some small localized regions cannot be excluded.

In any case, the physical explanation for the tight correlation between the HCN and IR is star formation in dense molecular gas. The active high-mass star-forming sites are the cores of GMCs, where the molecular gas is warmer and denser than in the GMC envelopes, where most of the CO emission originates. Currently, detailed statistical study examining the relationships among FIR, HCN, and CO on the scale of GMCs cores is not yet available. There are extensive observations (Plume et al. 1997) of another dense gas tracer, CS emission, of high-mass star formation cores in the Milky Way. All of these regions have an H_2 density more than sufficient to produce strong HCN emission.

4.2. Dense Molecular Gas and Star Formation Rates

For an initial mass function (IMF), typically taken to be the Salpeter IMF, $L_{\text{IR}}/M(\text{gas})$ can be interpreted as a measure of star formation efficiency (SFE), i.e., SFR per unit gas mass. This is because the SFR is related to L_{IR} by

$$\dot{M}_{\text{SFR}} \approx 2 \times 10^{-10} (L_{\text{IR}}/L_{\odot}) M_{\odot} \text{yr}^{-1}, \quad (9)$$

assuming that the observed FIR emission is produced primarily from dust heating by O, B, and A stars (e.g., Scoville & Young 1983; cf. Gallagher & Hunter 1987; Kennicutt 1998b). Although L_{IR} correlates with L_{CO} , the correlation is nonlinear, with a higher $L_{\text{IR}}/L_{\text{CO}}$ ratio for higher L_{IR} (Fig. 2b). On the other hand, L_{IR} linearly correlates with L_{HCN} , implying an almost constant SFR per unit of *dense* molecular gas mass for all galaxies.

The HCN luminosity can be related to the mass of dense gas, $M_{\text{dense}} = \alpha_{\text{HCN}} L_{\text{HCN}}$, if we assume the emission originates in the gravitationally bound cloud cores (see Paper I). For a volume-averaged core density $n(H_2) \sim 3 \times 10^4 \text{ cm}^{-3}$ and brightness temperature $T_b = 35 \text{ K}$, $\alpha_{\text{HCN}} = 2.1 \sqrt{n(H_2)}/T_b = 10 M_{\odot}/\text{K km s}^{-1} \text{ pc}^2$. Substituting in equation (1) gives a luminosity to dense gas mass ratio

$$L_{\text{IR}}/M_{\text{dense}} = 90 (\alpha_{\text{HCN}}/10) L_{\odot}/M_{\odot} \quad (10)$$

for all galaxies, although the mean is actually slightly higher ($\sim 120 L_{\odot}/M_{\odot}$) for the most luminous galaxies (see Table 2).

Combining equation (1) with equation (9), the SFR in terms of the HCN luminosity is

$$\dot{M}_{\text{SFR}} \approx 1.8 \times 10^{-7} (L_{\text{HCN}}/\text{K km s}^{-1} \text{ pc}^2) M_{\odot} \text{yr}^{-1}. \quad (11)$$

In terms of the dense gas mass, the star formation rate becomes

$$\dot{M}_{\text{SFR}} \approx 1.8 \left(\frac{M_{\text{dense}}}{10^8 M_{\odot}} \right) \left(\frac{10}{\alpha_{\text{HCN}}} \right) M_{\odot} \text{yr}^{-1}. \quad (12)$$

Since this is a linear relation, the HCN emission is a direct tracer of the SFR in all galaxies. The dense gas characteristic depletion time (half-life) is

$$\tau_{1/2} = 0.5 M_{\text{dense}} / \dot{M}_{\text{SFR}} \approx 2.7 \alpha_{\text{HCN}} \text{ Myrs}. \quad (13)$$

Although we adopted $\alpha_{\text{HCN}} \sim 10 M_{\odot}/\text{K km s}^{-1} \text{ pc}^2$ for normal spirals (Paper I), this conversion factor might be smaller for ULIGs as the T_b can be quite high (Downes & Solomon 1998), leading to shorter dense gas

depletion time-scales. HCN observations could potentially become one of the best SFR tracers in galaxies in the nearby and distant universe given the high sensitivity and the high spatial resolution achievable at millimeter wavelengths with the next generation of the millimeter telescopes.

There also appears to be some correlation between HCN emission and HCO^+ , CS, and other tracers of star formation, e.g., [C II] line emission and the FIR and 20cm continuum emission (Nguyen-Q-Rieu et al. 1992), although their sample is very limited. However, it has become clear that [C II] is underluminous in ULIGs (e.g., Luhman et al. 2003) and is not a consistent star formation indicator. In addition, in equation (9), it was assumed that most of the L_{IR} originates from star formation with little contribution from active galactic nuclei (AGNs) and/or from the general interstellar radiation field. It will be interesting to examine correlations between HCN and other indicators of star formation in a large sample of galaxies to assess which best indicates the SFR.

The tight correlation between the IR and HCN emission also implies that the dominant IR emission originates from the HCN emission region, especially in LIGs/ULIGs with concentrated molecular gas distribution. We know little of the size scales of the FIR emission regions in LIGs/ULIGs. The dominant contribution of the radio continuum and mid-IR emission in most LIGs appears to be from the inner regions (Condon et al. 1991; Telesco, Dressel, & Wolstencroft 1993; Hwang et al. 1999; Xu et al. 2000; Soifer et al. 2001). CO emission is usually concentrated in the inner regions, typically within a kpc of the center for ULIGs/LIGs (e.g., Scoville, Yun, & Bryant 1997; Downes & Solomon 1998; Sakamoto et al. 1999; Bryant & Scoville 1999; cf. Gao et al. 1999). HCN emission originates from the dense cores of the CO emitting regions, the sites of star formation, and the source of the FIR emission. Thus, we may predict the size scales and location of the FIR emission by determining the HCN source sizes from the HCN mapping.

4.3. The Global Star Formation Law

The IR–HCN linear correlation is valid over 3 orders of magnitude from low IR luminosity to the most luminous galaxies in the local universe. The direct consequence of the linear IR–HCN correlation is that the star formation law in terms of *dense* molecular gas content has a power-law index of 1.0. The global SFR is linearly proportional to the mass of the dense molecular gas (eq. [11] and Fig. 6). Parametrization in terms of observable mean surface densities of the dense molecular gas and the SFR will not change the slope of 1 in the IR–HCN correlation (SFR– M_{dense} correlation), or the linear power index of the star formation law, as both quantities are simply normalized by the same galaxy disk area. Our finding of an SFR proportional to the first power of the dense gas mass is different from the widely used star formation law with a slope of 1.4, derived by Kennicutt (1998a) for the disk-averaged SFR as a function of the total (HI and H_2) or just molecular gas surface density traced by CO emission. As we show below, this law is not valid for normal spiral galaxies and results only by combining normal galaxies with starburst galaxies and ULIGs.

4.3.1. Normal Spiral Galaxies

The IR–CO correlation (SFR– M_{H_2} correlation) is essentially linear up to luminosity $L_{\text{IR}} = 10^{11} \text{ L}_\odot$ (ULIGs and most LIGs excluded, see Fig. 1b). This seems to also be true in terms of the mean surface densities of the SFR and molecular gas mass for the nearest galaxies with spatially resolved observations (e.g., Wong & Blitz 2002; Rownd & Young 1999). The linear IR–CO correlation at low to moderate IR luminosity is expected since we find that the HCN–CO correlation is extremely tight and linear for normal

spiral galaxies (Fig. 3). Thus, the linear form of the global star formation law in terms of total molecular gas density as traced by CO for normal galaxies is due to the constant dense gas mass fraction indicated by the HCN/CO ratio (discussed in the next section). For normal star-forming spirals, the star formation law is linear in terms of both the total molecular gas and the dense molecular gas. Then how did Kennicutt (1998a) obtain a slope of 1.4 in the fitting of the star formation law? In our sample, a fit for the normal galaxies in the IR–CO correlation gives a slope of 1.0 (Fig. 1b), but this is not the case in Kennicutt’s normal galaxy sample, where there is a poor correlation between the SFR and the gas surface density. Thus, no reasonable slope can be derived from his normal galaxy sample alone.

4.3.2. All Galaxies: Normal Spiral, Starburst, and Ultraluminous Galaxies

A direct orthogonal regression fit of the IR–CO correlation for all galaxies in our sample (Fig. 1b) leads to a slope of 1.44. But the best-fitting least-squares slope (errors in L_{IR} only) is 1.27 (1.25 if galaxies with HCN limits are excluded, see §3.1). These fit slopes of the IR–CO correlation are almost identical to the star formation power-law index in Kennicutt’s (1998a) 36 circumnuclear starbursts and ULIG sample. It is obvious from Figure 1b that only galaxies with $L_{\text{IR}} > 10^{11} L_{\odot}$ (ULIGs and most LIGs) lie above the fixed line of slope 1. This combination of normal and very luminous galaxies leads to a fit with a power-law index of 1.4. Therefore, this slope is not a universal slope at all as it changes according to the sample selection. The 1.4 slope of the composite Schmidt law (Kennicutt’s Fig. 6, 1998a) is determined almost entirely from the starburst sample. The circumnuclear starbursts have some of the characteristics of ULIGs/LIGs. In particular, they must have a high dense gas fraction indicated by HCN/CO ratios (see section §4.4).

Indeed, when we add more LIGs/ULIGs into the sample for the IR–CO correlation, the slope becomes steeper. In Figure 7, we present an SFR– $M(H_2)$ (IR–CO) correlation diagram with an additional 40 galaxies, mostly ULIGs, with CO data from the literature (Solomon et al. 1997; Gao & Solomon 1999; Mirabel et al. 1990; Sanders et al. 1991), in addition to our HCN sample shown in Figure 1b. The least-squares fit gives a steep slope of 1.53, and the orthogonal regression fit leads to a much steeper slope of 1.73. In this sample luminous galaxies and normal galaxies have equal weight. It is clear that the ULIGs steepen the slope of the sample. There also appears to be a trend that some normal spirals with the lowest Σ_{SFR} and Σ_{H_2} in Kennicutt’s sample tend to lie below the 1.4 power fit line. Adding more extreme galaxies, both luminous ULIGs and low-luminosity spirals, tends to steepen the slope further toward 2. Therefore, it is difficult to derive a unique 1.4 power law based upon the total molecular gas or the total gas content.

The star formation rate in a galaxy depends linearly on the dense molecular gas content as traced by HCN, regardless of the galaxy luminosity or the presence of a “starburst”, and not the total molecular gas and/or atomic gas traced by CO and/or HI observations, respectively. Since dense molecular cloud cores are the sites of high-mass star formation, it is the physical properties, location, and mass of these cores that set the star formation rate. A detailed star formation law can be determined from observations directly probing the Milky Way cloud cores, particularly in the Milky Way molecular ring with spatially resolved measurements. The molecular tracers that best quantitatively indicate the presence of a starburst are primarily abundant molecules with high dipole moments such as HCN and CS requiring high molecular hydrogen density for excitation. The molecular property that best characterizes the star formation rate of a galaxy is the mass of dense gas. The gas density traced by HCN emission is apparently at or near the threshold for rapid star formation.

4.4. HCN/CO Ratio — A Better Indicator of Starbursts

Although HCN luminosity is a better indicator of star formation than CO in galaxies, it is very useful to compare the HCN with CO to obtain the HCN/CO ratio. The HCN/CO ratio is an indicator of the fraction of dense molecular gas available for vigorous star formation and gauges the globally averaged molecular gas density. The HCN/CO ratio is also a very successful predictor of starbursts (Fig. 4) and directly correlates with the SFE ($L_{\text{IR}}/L_{\text{CO}}$) (Fig. 5a). The SFE increases dramatically from *dense* molecular gas-poor galaxies to *dense* molecular gas-rich galaxies. The global luminosity ratio $L_{\text{HCN}}/L_{\text{CO}} = \langle \text{SBR} \rangle$ differs among galaxies of different luminosities (see Tables 1 & 2) with an average ratio of 1/6 for ULIGs and only 1/25 for normal spirals. *All galaxies in our sample with a global dense gas mass fraction $L_{\text{HCN}}/L_{\text{CO}} > 0.06$ are LIGs or ULIGs* (Fig. 4). We note that Curran et al. (2000) also find an average global ratio of 1/6 in luminous IR Seyfert galaxies, which they attribute to star formation.

The HCN/CO surface brightness ratio (SBR) is potentially a better and more practical indicator than the IR/CO ratio (the standard SFE diagnostic) of the starburst strength. Using the ratio IR/CO as a diagnostic, the IR emission is presumed to entirely originate from star formation. Other possible sources such as AGNs and the general interstellar radiation field are assumed to be negligible. The HCN/CO ratio instead is directly related to the molecular gas properties, particularly the local molecular gas density, which is tied to star formation. Moreover, the projection and confusion of different velocities along the line of sight is inevitably present in IR maps, whereas the different velocity components can be distinguished from the kinematics obtained in the detailed CO and HCN maps. In addition, the low spatial resolution available in the FIR, even with the *Spitzer Space Telescope* and the upcoming *SOFIA*, and other future far-IR space missions, is incompatible with the high resolution available from millimeter interferometers. Therefore, it is important to map the HCN/CO ratio in galaxies in order to fully explore the star formation properties and SFE.

As we show elsewhere from HCN maps of nearby galaxies (Gao 1996; Y. Gao & P.M. Solomon 2004, in preparation), the ratio of $I_{\text{HCN}}/I_{\text{CO}}$, i.e., the surface brightness ratio (SBR), in most cases, is high in the centers of spiral galaxies and typically drops off at large galactic radii. A significant fraction of dense molecular gas is (traced by HCN emission) distributed in the inner disks of galaxies outside the nuclear or inner ring starburst regions and can be detected to radii as large as a few kpc, perhaps to diameters of $\sim D_{25}/4$. We find the highest fraction of dense molecular gas, indicated by the SBR (as measured by single-dish telescopes with beam sizes ~ 1 kpc),

$$\text{SBR (cores)} \equiv I_{\text{HCN}}/I_{\text{CO}} \text{ (cores)} \approx 0.1, \quad (14)$$

nearly comparable to those observed globally from ULIGs, in the centers of most normal spiral galaxies observed (usually the nuclear starburst cores). We attribute this to the presence of a starburst. Helfer & Blitz (1993, 1997a) found similarly high ratios in the centers of normal galaxies, which they relate to the high ambient pressure, but they do not correlate their data with infrared luminosity or star formation rates.

We also find that the SBR ratio generally falls off in the disks at larger radii (e.g., $\gtrsim 3$ kpc), to a very low SBR ~ 0.015 –0.03. This low SBR (disks) $\lesssim 0.03$ is the same as that found in the Milky Way’s disk on average, and over the full extent of nearby GMCs in the Milky Way (Helfer & Blitz 1997b), as well as outside the central regions in several normal spiral galaxies mapped with an interferometer (Helfer & Blitz 1997a).

Although the *global* luminosity ratio $L_{\text{HCN}}/L_{\text{CO}} = \langle \text{SBR} \rangle$ differs dramatically among galaxies of different luminosities (see Tables 1 & 2), the difference between the SBR in central beam measurements

of galaxies is related to the different telescope beam diameters (e.g., Helfer & Blitz 1993), different source sizes (of CO and HCN), and different size scales of the starburst cores in the centers of individual galaxies. The CO/HCN intensity ratio (the inverse of SBR) changes from 20 – 80 for normal spiral galaxies to 4 – 10 for ULIGs. However, if only central beam measurements are used, the ratio seems quite uniform (Aalto et al. 1995). The central beam measurement is not representative of the global measurement (of the entire galaxy) and may not even be an accurate measurement of the central region since it is telescope dependent. This explains why Aalto et al. (1995) did not find the strong $L_{\text{IR}}-L_{\text{HCN}}$ correlation.

The distribution of the HCN emission, particularly HCN/CO ratio maps, can be used directly to locate starburst sites in nearby galaxies. High-resolution maps of HCN and HCN/CO have been obtained in the central regions of a few nearby normal galaxies, some with clear central starbursts. Paglione et al. (1995) mapped the central bar in the starburst nucleus of NGC 253 and found a peak HCN/CO=0.2 falling off to 0.04 at a galactocentric radius of 200 pc. The peak SBR in this starburst is similar to the global value in the most luminous galaxies in our sample (Fig. 4). Both the strongest HCN surface brightness and the strongest SBR occurred at the location of strong, extended nonthermal radio continuum and thermal free-free emission associated with the starburst. Using our Figure 5a, this high SBR (0.15–0.2) indicates that this small central starburst has an $L_{\text{IR}}/L_{\text{CO}}$ ratio comparable to that of ULIGs, $L_{\text{IR}}/L_{\text{CO}} \sim 200L_{\odot}/\text{Kkm s}^{-1}\text{pc}^2$. Unfortunately, there are no high-resolution IR observations available to test this prediction. Paglione et al. (1995) estimated the L_{IR} from the radio continuum to be $L_{\text{IR}} \sim 1 \times 10^9L_{\odot}$. The L_{CO} estimated from the HCN and HCN/CO ratios is approximately $4 \times 10^7\text{Kkm s}^{-1}\text{pc}^2$ yielding a rough $L_{\text{IR}}/L_{\text{CO}} \sim 250L_{\odot}/\text{Kkm s}^{-1}\text{pc}^2$, in agreement with the prediction of Figure 5a.

High HCN/CO ratios (0.1–0.2) are also found in the central $\lesssim 1$ kpc regions of several other galaxies (Downes et al. 1992; Helfer & Blitz 1997a; Reynaud & Downes 1997; Kohno et al. 1996; Kohno, Kawabe, & Vila-Vilaro 1999). Kohno et al. (1999) found that most of the HCN emission, as well as an enhanced HCN/CO ratio, is associated with the circumnuclear star-forming ring in NGC 6951. No significant enhancement of the HCN/CO ratio is observed at the CO peaks. In IC 342 with a resolution of 60 pc⁴ (Downes et al. 1992), however, only three of five HCN clouds seem to be actively forming into stars based on the presence of free-free emission. However, the observations of the free-free emission are still of limited sensitivities, either at 2cm and 6cm (Turner & Ho 1983; Turner et al. 1993) or at 3 mm (Meier & Turner 2001). And there are no high-resolution FIR observations available to clearly indicate the star formation activities and star formation rates at this small scale. Judging from all these observations and the $H\alpha$ emission (Turner & Hurt 1992), there is probably star formation in all the HCN clouds (D. Downes 2003, private communication). Are some of these HCN clouds precursors to a starburst? Although the HCN/CO ratios are high (~ 0.14) for these HCN clouds, the average of a several hundred parsec central region has only an HCN/CO ratio of $\lesssim 0.05$ in IC 342, clearly not a strong starburst.

A recent summary of the HCN/CO ratios obtained in six central nuclear starbursts (Shibatsuka et al. 2003) lists a typical ratio $\text{HCN/CO} \approx 0.1-0.25$. Sorai et al. (2002) also find the highest HCN/CO ratio of ~ 0.1 in central regions of a few nearby galaxies. This is the same as the global ratio we find in many LIGs and all ULIGs that have HCN luminosities several hundred times greater than the central starbursts of normal galaxies.

The only LIGs that have been well imaged in HCN are the AGN/starburst hybrid galaxy NGC 1068 (Tacconi et al. 1997, 1994; Helfer & Blitz 1995; Jackson et al. 1993), which has very high HCN/CO ratio

⁴Distance to IC 342 is adopted as 3.7 Mpc, see Table 1.

($\gtrsim 0.3$) within ~ 100 pc nuclear region, the merging pair Arp 299 (Aalto et al. 1997; Casoli et al. 1999), and the archetypal ULIG Arp 220 (Radford et al. 1991; N. Z. Scoville 2001, private communication). Arp 299 may harbor an AGN in the eastern nucleus (e.g., Gehrz et al. 1983), similar to NGC 1068. It appears that some weak Seyferts also have rather high HCN/CO ratio ($\gtrsim 0.2$) in the innermost $\lesssim 100$ pc nuclear region around the AGN (e.g., M51, Kohno et al. 1996). But this contributes little to the average HCN/CO ratios in the circumnuclear (~ 0.5 –1 kpc) starburst rings where most of the molecular gas is located.

Ultimately, it is the dense molecular gas, rather than the total molecular gas content, that is the raw material for active star formation in galaxies. Our global measurements of 65 galaxies show that the dense molecular gas fraction indicated by $L_{\text{HCN}}/L_{\text{CO}}$ is an important measure of the star formation efficiency; the mass of dense molecular gas indicated by L_{HCN} is a very good measure of the star formation rate deduced from L_{IR} . The total molecular content indicated by L_{CO} is an unreliable indicator of star formation rate particularly in starburst galaxies. The location of starburst regions and better characterization of the starbursts in individual galaxies could be better indicated by the local SBR measurements, obtained by the high-resolution and high-sensitivity HCN and CO observations.

4.5. Starburst Origin of the Far-IR Emission

Our results show that high-mass star formation in dense molecular gas is responsible for the infrared luminosity from a wide range of galaxies including normal spirals of moderate IR luminosity ($5 \times 10^9 L_{\odot} \lesssim L_{\text{IR}} \lesssim 10^{11} L_{\odot}$), luminous infrared galaxies (LIGs, $10^{11} L_{\odot} \lesssim L_{\text{IR}} \lesssim 10^{12} L_{\odot}$), and ultraluminous galaxies (ULIGs, $L_{\text{IR}} \gtrsim 10^{12} L_{\odot}$). The star formation rate or IR luminosity is proportional to the mass of dense molecular gas in all galaxies.

4.5.1. Luminous and Ultraluminous Infrared Galaxies

Evidence is mounting that the dominant energy source in most ULIGs is from the extreme starbursts rather than the dust-enshrouded AGNs (e.g., Solomon et al. 1997; Downes & Solomon 1998; Genzel et al. 1998; Scoville et al. 2000; Soifer et al. 2001). The debate about the energy source in ULIGs, particularly in “warm” ULIGs, has been going on for over a decade (e.g., Sanders et al. 1988; Veilleux et al. 1999; Sanders 1999; Joseph 1999). Although AGNs are present in many ULIGs (e.g., Nagar et al. 2003; Franceschini et al. 2003), there is little evidence indicating that the AGN contribution is the dominant source of the FIR emission.

Our results summarized in § 3 provide compelling evidence in favor of a star formation origin for the huge infrared luminosity from ultraluminous galaxies. We have shown that the infrared luminosity of all molecular gas-rich spiral galaxies including ULIGs is proportional to the dense star-forming molecular gas mass traced by L_{HCN} (see Fig. 1a and Fig. 6).

One of the main arguments in favor of an AGN as the power source in ULIGs is the anomalously high ratio $L_{\text{IR}}/L_{\text{CO}}$ or $L_{\text{IR}}/\text{M}(\text{H}_2)$. The IR luminosity and thus the required star formation rate per solar mass of molecular gas (as traced by CO emission) is an order of magnitude higher in ultraluminous and most luminous galaxies than in normal spiral galaxies, suggesting that an AGN rather than star formation is required (Sanders et al. 1988, 1991) in order to produce the high infrared emission. Viewed in terms of the dense gas mass the situation is completely different. The ratio $L_{\text{IR}}/L_{\text{HCN}}$ or $L_{\text{IR}}/\text{M}_{\text{dense}}$ is essentially the

same in all galaxies including ULIGs. Figure 8 shows that $L_{\text{IR}}/\text{M}_{\text{dense}}$ is virtually independent of galaxy luminosity and on average $L_{\text{IR}}/\text{M}_{\text{dense}} = 90\text{L}_{\odot}/\text{M}_{\odot}$, about the same as in molecular cloud cores but much higher than in GMCs as a whole (Mooney & Solomon 1988). Ultraluminous galaxies simply have a large quantity of dense molecular gas and thus produce a prodigious starburst that heats the dust. It is not surprising that starbursts of this magnitude are observed in the infrared and never seen in the optical-UV part of the spectrum. The young OB stars are imbedded in very massive and dense regions dwarfing anything found in Milky Way GMCs and all of their optical-UV radiation is absorbed by dust. Although ULIGs are not simply scaled-up versions of normal spirals in terms of their total molecular mass, they are scaled-up versions in terms of their dense molecular gas mass, which is exactly what is expected if star formation is the power source.

Ultimately, even for warm ULIGs (e.g., Surace et al. 1998), which might have, to some degree, evolved into the phase of the dust-enshrouded QSOs/AGNs (e.g., Sanders et al. 1989; Surace & Sanders 1999; Veilleux et al. 1999; Genzel et al. 1998; Sanders 1999), we may still be able to tell whether starbursts still dominate most of the high L_{IR} or not by examining their total dense molecular gas content and the fraction of dense molecular gas. For instance, *IRAS* 05189-2524 and Mrk 231 are warm ULIGs, but they have similar $L_{\text{IR}}/\text{M}_{\text{dense}}$ and HCN/CO ratio as the other seven out of nine ULIGs in our sample. Clearly, more HCN observations are required to judge if warm ULIGs distinguish themselves from other ULIGs.

4.5.2. Normal Spiral Galaxies

Although some fraction of L_{IR} originates from outer disks in nearby large spiral galaxies, the dominant contribution is still from the centers (e.g., Rice et al. 1988). Better resolution *IRAS* maps, obtained by an improved imaging deconvolution algorithm, tend to show much more centrally concentrated FIR emission in the inner disks (Rice 1993). Devereux & Young (1990) have shown that the global FIR luminosity in spiral galaxies is consistent with that contributed by warm dust heating from the high-mass OB stars. Higher resolution (as compared with that of *IRAS*) measurements of the 160 μm and H α emission in nearby galaxies NGC 6946 and M51 suggest that the FIR luminosity is in quantitative agreement with that expected from OB stars throughout the star-forming disks (Devereux & Young 1992, 1993).

The existence of cold dust components of $\lesssim 30$ and $\lesssim 20$ K in nearby galaxies has been revealed from both recent ISOPHOT FIR observations (e.g., Popescu et al. 2004; Haas et al. 1998; Alton et al. 1998a; Davies et al. 1999) and SCUBA submillimeter observations (e.g., Alton et al. 1998b; 2000), respectively. The cold dust distribution usually has a larger radial extent (e.g., Alton et al. 1998a) and the dominant cold dust component may not be closely associated with the active star-forming inner disks. HCN maps of nearby galaxies (e.g., Nguyen-Q-Rieu et al. 1992; Helfer & Blitz 1997a; Y. Gao & P.M. Solomon 2004, in preparation) show that the HCN emission region is much more compact than that of CO emission region in normal spiral galaxies and/or starburst galaxies and is thus closely related to the warm dust in the inner disks.

The contribution of the general interstellar radiation field to the total FIR emission in galaxies might be significant at the low- L_{IR} end, where the general infrared interstellar radiation field is comparable to the IR radiation from the active star formation. This might be testable on the IR-HCN correlation plot (Fig. 1a) for galaxies of the lowest L_{IR} ($\lesssim 5 \times 10^9\text{L}_{\odot}$) when more observations of the lowest L_{IR} sources are available to show a statistically significant trend. Given that the tight correlation between these two quantities might be used to predict one another, one can check whether low- L_{IR} galaxies have a higher

$L_{\text{IR}}/L_{\text{HCN}}$ than expected from the IR–HCN correlation.

4.6. High Redshift Galaxies and AGN

AGNs may become more important than star formation at the very high IR luminosity end, especially in warm ULIGs (Veilluex et al. 2003), in contributing the bulk of the energy output (e.g., Sanders et al. 1988; Veilluex et al. 1999). For extremely luminous galaxies with $L_{\text{IR}} \sim 10^{13} L_{\odot}$, the so-called hyperluminous infrared galaxies (HLIGs, Sanders & Mirabel 1996; Rowan-Robinson 2000), the implied SFR (Equation 9) would be $\sim 2000 M_{\odot} \text{yr}^{-1}$. Although such super-starburst galaxies likely exist at high redshifts and HLIGs could indeed be such super-starburst systems (if the magnification by a gravitational lens and the AGN contribution to the IR emission are not important), there are no similar systems in the local universe.

If the tight correlations obtained from our local HCN sample are applicable to high- z galaxies, we can roughly estimate their expected molecular gas properties. For the whole sample $L_{\text{IR}}/L_{\text{HCN}} = 900 L_{\odot}/\text{Kkm s}^{-1}\text{pc}^2$ (Equation 1). But ULIGs have a slightly higher ratio of $L_{\text{IR}}/L_{\text{HCN}} = 1200 L_{\odot}/\text{Kkm s}^{-1}\text{pc}^2$ (Table 2). For high- z galaxies with $L_{\text{IR}} \sim 10^{13} L_{\odot}$, we thus expect to have $L_{\text{HCN}} \sim 0.8 \times 10^{10} \text{Kkm s}^{-1}\text{pc}^2$ if they are the analogs of local ULIGs. This is only a factor of 2–3 higher than the highest L_{HCN} observed in local ULIGs. The first high- z HCN detection is from the Cloverleaf quasar at $z=2.567$, helped by the magnification of the gravitational lens, with the intrinsic, magnification-corrected $L_{\text{HCN}} \sim 0.3 \times 10^{10} \text{Kkm s}^{-1}\text{pc}^2$ (Solomon et al. 2003). It appears that, if the hot dust AGN component can be subtracted from the total IR emission, then even the Cloverleaf quasar seems to fit the IR–HCN correlation determined here from the local universe.

At present, more than 20 CO sources at high z have been detected, all with high CO luminosity (e.g., Cox et al. 2002; Carilli et al. 2002; Papadopoulos et al. 2001; Guilloteau et al. 1999; Downes et al. 1999; Frayer et al. 1998). We can estimate the expected L_{HCN} for these extraordinarily large L_{CO} sources detected at high z using our HCN–CO correlation (Fig. 3). Cox et al. (2002) report the strongest CO emitter detected to date, with $L_{\text{CO}} \sim 10^{11} \text{Kkm s}^{-1}\text{pc}^2$ even after the magnification by the gravitational lensing is corrected. Using Equation 2, or $L_{\text{HCN}}/L_{\text{CO}} = 0.1 \times (L_{\text{CO}}/10^{10} \text{Kkm s}^{-1}\text{pc}^2)^{0.38}$, we obtain $L_{\text{HCN}} \sim 2.4 \times 10^{10} \text{Kkm s}^{-1}\text{pc}^2$ and $L_{\text{HCN}}/L_{\text{CO}} = 0.24$. This $L_{\text{HCN}}/L_{\text{CO}}$ ratio is the same as the very highest found for local ULIGs. For this largest L_{CO} source, $L_{\text{IR}} \sim 2.0 \times 10^{13} L_{\odot}$ is estimated by Cox et al. (2002) based on the 250 and 350 GHz measurements (Omont et al. 2001; Isaak et al. 2002). And using $L_{\text{IR}}/L_{\text{HCN}} = 1200 L_{\odot}/\text{Kkm s}^{-1}\text{pc}^2$, we expect to have $L_{\text{HCN}} = 1.7 \times 10^{10} \text{Kkm s}^{-1}\text{pc}^2$. Perhaps a better estimate of the expected HCN luminosity can be constrained from both IR and CO luminosities by using the multiparameter fit from equation (4). Indeed, we also obtain $L_{\text{HCN}} = 1.7 \times 10^{10} \text{Kkm s}^{-1}\text{pc}^2$. If such high L_{HCN} is eventually detected in this source, then star formation rather than AGNs must be responsible for most of the high infrared luminosity.

We can also roughly estimate the expected upper limit of $L_{\text{IR}}/L_{\text{CO}}$ for HLIGs and/or high- z galaxies, if they are powered by star formation and the correlation between $L_{\text{IR}}/L_{\text{CO}}$ and $L_{\text{HCN}}/L_{\text{CO}}$ found in Figure 5a is applicable. Although there are very large scatters (~ 0.5 dex, 2σ) in the fit, this should be good to within a factor of ~ 3 . Here we can take $L_{\text{HCN}}/L_{\text{CO}} \lesssim 1$ as upper limits. Using the orthogonal fit $\log L_{\text{IR}}/L_{\text{CO}} = 1.24 \log L_{\text{HCN}}/L_{\text{CO}} + 3.24$, we obtain $L_{\text{IR}}/L_{\text{CO}} \lesssim 1700 L_{\odot}/\text{Kkm s}^{-1}\text{pc}^2$. Therefore, the expected maximum L_{IR} from star formation is always less than $\lesssim 1.7 \times 10^{14} (L_{\text{CO}}/10^{11} \text{Kkm s}^{-1}\text{pc}^2) L_{\odot}$.

Although many submillimeter galaxies are HLIGs, few have $L_{\text{IR}} \sim 10^{14} L_{\odot}$ (Chapman et al. 2003). The highest L_{CO} detected among submillimeter galaxies is $\sim 0.7 \times 10^{11} \text{Kkm s}^{-1}\text{pc}^2$ (Neri et al. 2003; Greve,

Ivison, & Papadopoulos 2003). If any sources indeed have high $L_{\text{HCN}} \sim 0.7 \times 10^{11} \text{ K km s}^{-1} \text{ pc}^2$, it appears that extreme starbursts from abundant active star-forming dense molecular gas are still possible to power such $L_{\text{IR}} \sim 10^{14} L_{\odot}$ sources. This corresponds roughly to the maximum possible SFR of $\sim 2 \times 10^4 M_{\odot}/\text{yr}$ (using eq. [9]), as argued by Heckman (2000) based on physical causality for self-gravitating, extremely massive galaxy systems of $\sim 10 \times L_{*}$. Observing HCN in addition to CO will help distinguish whether star formation rather than AGNs contributes mostly to the highest L_{IR} observed.

5. SUMMARY

HCN luminosity is a tracer of *dense* molecular gas, $n(H_2) \gtrsim 3 \times 10^4 \text{ cm}^{-3}$, associated with star-forming molecular cloud cores. Here we briefly summarize the principal results found from an analysis of our HCN survey of galaxies:

1. A tight linear correlation between the IR and HCN luminosities L_{IR} and L_{HCN} in 65 galaxies is established with a correlation coefficient $R=0.94$ (Fig. 1a). There is also a significant correlation between the normalized luminosities $L_{\text{IR}}/L_{\text{CO}}$ and $L_{\text{HCN}}/L_{\text{CO}}$ which confirms the true physical relationship between L_{IR} and L_{HCN} . The IR–HCN linear correlation is valid over 3 orders of magnitude including ultraluminous infrared galaxies, the most luminous galaxies in the local universe. The direct consequence of the linear IR–HCN correlation is that the star formation law in terms of *dense* molecular gas content has a power law index of 1.0. The global star formation rate is linearly proportional to the mass of dense molecular gas in normal spiral galaxies, luminous infrared galaxies and ultraluminous infrared galaxies. This is strong evidence in favor of star formation as the power source in ultraluminous infrared galaxies since the star formation in these galaxies appears to be normal and expected given their high mass of dense star-forming gas.

2. The star formation rate indicated by L_{IR} depends on the amount of dense molecular gas traced by HCN emission, not the total molecular gas traced by CO emission. One of the main arguments in favor of an AGN (Sanders et al. 1988) as the power source in ultraluminous infrared galaxies is the anomalously high ratio $L_{\text{IR}}/L_{\text{CO}}$ or $L_{\text{IR}}/M(H_2)$. The IR luminosity and thus the required star formation rate per solar mass of molecular gas traced by CO emission, is an order of magnitude higher in ultraluminous infrared galaxies and most luminous infrared galaxies than in normal spiral galaxies. This has been interpreted as indicating that a dust enshrouded AGN rather than star formation is required to produce the very high luminosity (Sanders et al. 1991). Viewed in terms of the dense gas mass the situation is completely different. The ratio $L_{\text{IR}}/L_{\text{HCN}}$ or $L_{\text{IR}}/M_{\text{dense}}$ is the same in all galaxies including ultraluminous infrared galaxies. Figure 8 shows that $L_{\text{IR}}/M_{\text{dense}}$ is virtually independent of galaxy luminosity and on average $L_{\text{IR}}/M_{\text{dense}} \approx 90 L_{\odot}/M_{\odot}$, about the same as in molecular cloud cores but much higher than in GMCs as a whole (Mooney & Solomon 1988). Ultraluminous infrared galaxies simply have a large quantity of dense molecular gas and thus produce a prodigious starburst which heats the dust, produces the IR, and blocks all or most optical radiation. Although ultraluminous infrared galaxies are not simply scaled up versions of normal spirals in terms of their total molecular mass they are scaled up version in terms of their dense molecular gas mass, which is exactly what is expected if star formation is the power source. We note that our sample includes 9 ultraluminous infrared galaxies ($L_{\text{IR}} > 0.8 \times 10^{12} L_{\odot}$) and 23 luminous infrared galaxies ($L_{\text{IR}} > 10^{11} L_{\odot}$) but only 2 “warm” ultraluminous infrared galaxies (Surace et al. 1998), a subclass representing about 25% of all ultraluminous infrared galaxies. Although these 2 warm ultraluminous infrared galaxies appear normal in terms of the IR/HCN ratio, further investigation of warm ultraluminous infrared galaxies is required.

3. The HCN/CO ratio is an indicator of the fraction of dense molecular gas available for vigorous star formation and gauges the globally averaged molecular gas density. It is a powerful starburst indicator.

There is a strong correlation between the HCN and CO luminosities in galaxies although the correlation is not linear. The ratio $L_{\text{HCN}}/L_{\text{CO}}$ is constant for normal spirals and increases for luminous and ultraluminous IR galaxies. The global ratio $L_{\text{HCN}}/L_{\text{CO}} = \langle \text{SBR} \rangle$ (see Tables 1 & 2) has an average ratio of 1/6 for ultraluminous infrared galaxies and only 1/25 for normal spirals. The HCN/CO ratio is a very successful predictor of starbursts (Fig. 4) and directly correlates with the star formation efficiency indicator ($L_{\text{IR}}/L_{\text{CO}}$) (Fig. 5a). The SFE increases dramatically from *dense* molecular gas-poor galaxies to *dense* molecular gas-rich galaxies. *All galaxies in our sample with a high dense gas mass fraction indicated by $L_{\text{HCN}}/L_{\text{CO}} > 0.06$ are luminous or ultraluminous infrared galaxies* (Fig. 4).

4. The correlation between L_{IR} and L_{CO} may be a consequence of the stronger correlations between L_{IR} and L_{HCN} and between L_{HCN} and L_{CO} . A model two parameter fit for $L_{\text{IR}}(L_{\text{HCN}}, L_{\text{CO}})$ shows almost no dependence on L_{CO} . Much of the CO emission originates from moderate density regions with low to moderate dust temperature and little or no active high mass star formation. A critical molecular parameter that measures star formation rates in galaxies is the amount of dense molecular gas measured by the HCN luminosity. High molecular gas density, strong HCN emission and warm dust heated by the newly formed OB stars go together.

5. A quantitative star formation theory must start with the processes that form dense cloud cores, particularly massive cores. It appears from our survey of 65 IR/CO bright galaxies including normal spirals and very luminous IR starbursts that once the local density is raised from that of a typical GMC ($n(H_2) \sim$ a few $\times 10^2 \text{ cm}^{-3}$) to $3 \times 10^4 \text{ cm}^{-3}$, star formation including high-mass star formation is efficient and progresses rapidly. The characteristic time scale for using half of all the dense gas is about 2×10^7 years.

Many thanks are owed to Judy Young for helpful discussions and suggestions. We appreciate the generous support and allocation of observing time from the NRAO 12m, IRAM 30m, and FCRAO 14m telescopes. We also thank the anonymous referee for a careful and helpful report. This research has made use of the NASA/IPAC Extragalactic Database (NED), which is operated by the Jet Propulsion Laboratory, Caltech, under contract with the National Aeronautics and Space Administration.

Table 1. Global Properties of Galaxies in the HCN Survey^a

Galaxies	D_L Mpc	L_{IR} $10^{10} L_{\odot}$	L_{CO} $10^8 \text{ Kkm s}^{-1} \text{pc}^2$	$L_{\text{HCN}}^{\text{b}}$ >0.26	$L_{\text{HCN}}/L_{\text{CO}}$ <SBR>	$L_{\text{IR}}/L_{\text{HCN}}$ $L_{\odot}/\text{Kkm s}^{-1} \text{pc}^2$	$T_{\text{dust}}^{\text{c}}$ K
NGC 253	2.5	2.1	4.6	0.27	0.059	778	34
IC 1623	81.7	46.7	130.5	8.5	0.065	549	39
NGC 660	14.0	3.7	7.3	>0.26	>0.036	<1420	37
NGC 695	133.5	46.6	92.9	4.3	0.046	1080	34
MRK 1027	123.5	25.7	41.7	1.89	0.045	1350	37
NGC 891	10.3	2.6	11.0	0.25	0.024	1120	28
NGC 1022	21.1	2.6	4.2	0.20	0.047	1300	39
NGC 1055	14.8	2.1	13.3	<0.37	<0.028	>568	29
NGC 1068	16.7	28.3	20.7	3.61	0.174	784	40
NGC 1144	117.3	25.1	108.9	2.67	0.025	940	32
NGC 1365	20.8	12.9	58.7	3.10	0.053	420	32
IC 342	3.7	1.4	9.5	0.47	0.050	300	30
NGC 1614	63.2	38.6	24.5	1.25	0.051	3090	46
*VIZW31	223.4	87.1	125.0	9.8	0.078	890	34
*05189-2524	170.3	118.1	67.0	6.2	0.093	1900	48
NGC 2146	15.2	10.0	12.5	0.96	0.071	1040	38
NGC 2276	35.5	6.2	10.2	0.40	0.039	1550	31
ARP 55	162.7	45.7	125.0	3.8	0.030	1200	36
NGC 2903	6.2	0.83	2.3	>0.09	>0.036	< 922	29
*UGC 05101	160.2	89.2	50.8	10.0	0.197	892	36
M82	3.4	4.6	5.7	0.30	0.053	1530	45
NGC 3079	16.2	4.3	24.0	~1.0	~0.042	~430	32
*10566+2448	173.3	93.8	61.5	10.2	0.166	920	42
ARP 148	143.3	36.5	>47.0	4.0	<0.085	913	35
NGC 3556	10.6	1.35	>4.5	>0.09	~0.020	<1500	30
NGC 3627	7.6	1.26	4.4	>0.08	>0.017	<1580	30
NGC 3628	7.6	1.01	7.1	0.24	0.034	421	30
NGC 3893	13.9	1.15	4.1	0.23	0.056	500	30
NGC 4030	17.1	2.14	15.2	0.54	0.036	398	29
NGC 4041	18.0	1.70	3.9	0.18	0.046	944	31
NGC 4414	9.3	0.81	4.6	0.16	0.033	510	29
NGC 4631	8.1	2.0	2.3	~0.08	~0.037	~2380	30
NGC 4826	4.7	0.26	1.3	>0.04	>0.030	<750	33
NGC 5005	14.0	1.4	8.2	0.41	0.049	350	28
NGC 5055	7.3	1.1	8.6	>0.10	>0.012	<1140	26
NGC 5135	51.7	13.8	31.3	2.73	0.087	510	36
M83	3.7	1.4	8.1	0.35	0.043	420	31
*MRK 273	152.2	129.9	65.0	15.2	0.234	860	48

Table 1—Continued

Galaxies	D_L Mpc	L_{IR} $10^{10} L_\odot$	L_{CO} $10^8 \text{ Kkm s}^{-1} \text{pc}^2$	$L_{\text{HCN}}^{\text{b}}$ $10^8 \text{ Kkm s}^{-1} \text{pc}^2$	$L_{\text{HCN}}/L_{\text{CO}}$ <SBR>	$L_{\text{IR}}/L_{\text{HCN}}$ $L_\odot/\text{Kkm s}^{-1} \text{pc}^2$	$T_{\text{dust}}^{\text{c}}$ K
NGC 5678	27.8	3.0	17.2	0.75	0.044	410	29
NGC 5713	24.0	4.2	8.1	0.22	0.027	1880	27
NGC 5775	21.3	3.8	10.9	0.57	0.052	670	32
*17208-0014	173.1	234.5	146.9	37.6	0.256	640	46
18293-3413	72.1	53.7	85.5	4.03	0.047	1330	38
NGC 6701	56.8	11.2	34.0	1.38	0.041	820	32
NGC 6921	60.3	11.4	17.5	~2.81	~0.160	~410	34
NGC 6946	5.5	1.6	9.2	0.49	0.053	330	30
NGC 7130	65.0	21.4	44.9	3.27	0.071	660	37
IC 5179	46.2	14.1	~26.4	3.42	~0.129	420	33
NGC 7331	15.0	3.5	>10.7	>0.44	~0.041	<800	28
NGC 7469	67.5	40.7	37.1	2.19	0.059	1860	41
NGC 7479	35.2	7.4	26.7	1.12	0.042	665	36
*23365+3604	266.1	142.0	85.0	15.0	0.176	950	45
MRK 331	75.3	26.9	52.1	3.35	0.064	810	41
Literature HCN Data							
*MRK 231	170.3	303.5	82.2	18.6	0.226	1630	47
*ARP 220	74.7	140.2	78.5	9.2	0.117	1520	44
NGC 6240	98.1	61.2	79.0	11.0	0.139	560	41
ARP 193	92.7	37.3	39.8	9.5	0.238	400	37
ARP 299	43.0	62.8	29.0	2.1	0.072	2990	46
NGC 7771	60.4	21.4	90.8	6.5	0.070	335	33
NGC 828	75.4	22.4	58.5	1.3	0.022	1720	33
NGC 520	31.1	8.5	16.3	0.64	0.039	1330	38
NGC 3147	39.5	6.2	59.0	0.90	0.015	690	26
NGC 1530	35.4	4.7	23.0	0.49	0.021	960	29
NGC 4945	3.7	2.6	5.8	~0.27	~0.047	~960	31
M51	9.6	4.2	19.4	0.50	0.026	850	30

^aThis table contains all HCN Survey data of Gao & Solomon (2003, Paper I) and includes a dozen galaxies in the literature (almost entirely from Solomon et al. 1992, but M51 and NGC 4945 from Nguyen-Q-Rieu et al. 1992 and Henkel et al. 1994, respectively). LIGs with $L_{\text{IR}} > 10^{11} L_\odot$ are in boldface, and ULIGs with $L_{\text{IR}} \gtrsim 10^{11.9} L_\odot$ are further marked with an asterisk ().

^bThe 2σ upper limit (<) is listed for NGC 1055. The lower limits (>) are for nearby galaxies, where we only detected HCN in the galaxy centers or more extensive mapping is still required.

^cThe warm dust temperature T_{dust} is for optical thin dust with emissivity $\sim \nu^\beta$, $\beta = 1.5$.

Table 2. Summary of the Average IR, CO and HCN Luminosities

L_{IR} L_{\odot}	No. ¹ of galaxies	L_{HCN} $10^8 \text{ Kkm s}^{-1} \text{pc}^2$	L_{CO} $10^8 \text{ Kkm s}^{-1} \text{pc}^2$	$L_{\text{IR}}/L_{\text{CO}}$ $L_{\odot}/\text{Kkm s}^{-1} \text{pc}^2$	$L_{\text{IR}}/L_{\text{HCN}}$ $L_{\odot}/\text{Kkm s}^{-1} \text{pc}^2$	$L_{\text{CO}}/L_{\text{HCN}}^2$
Normal $< 10^{11}$	26	0.35	8.7	30	740	25
$10^{11} < \text{LIGs} \lesssim 0.8 \times 10^{12}$	22	3.1	47.6	60	890	14
ULIGs $\gtrsim 10^{11.9}$	9	9.0	69.0	170	1200	6
All	57	1.5	20.0	50	870	17

¹Galaxies with only limits in HCN luminosity are excluded.

²The inverse of average surface brightness ratio $\langle \text{SBR} \rangle \equiv L_{\text{HCN}}/L_{\text{CO}}$ indicating the fraction of dense molecular gas in galaxies.

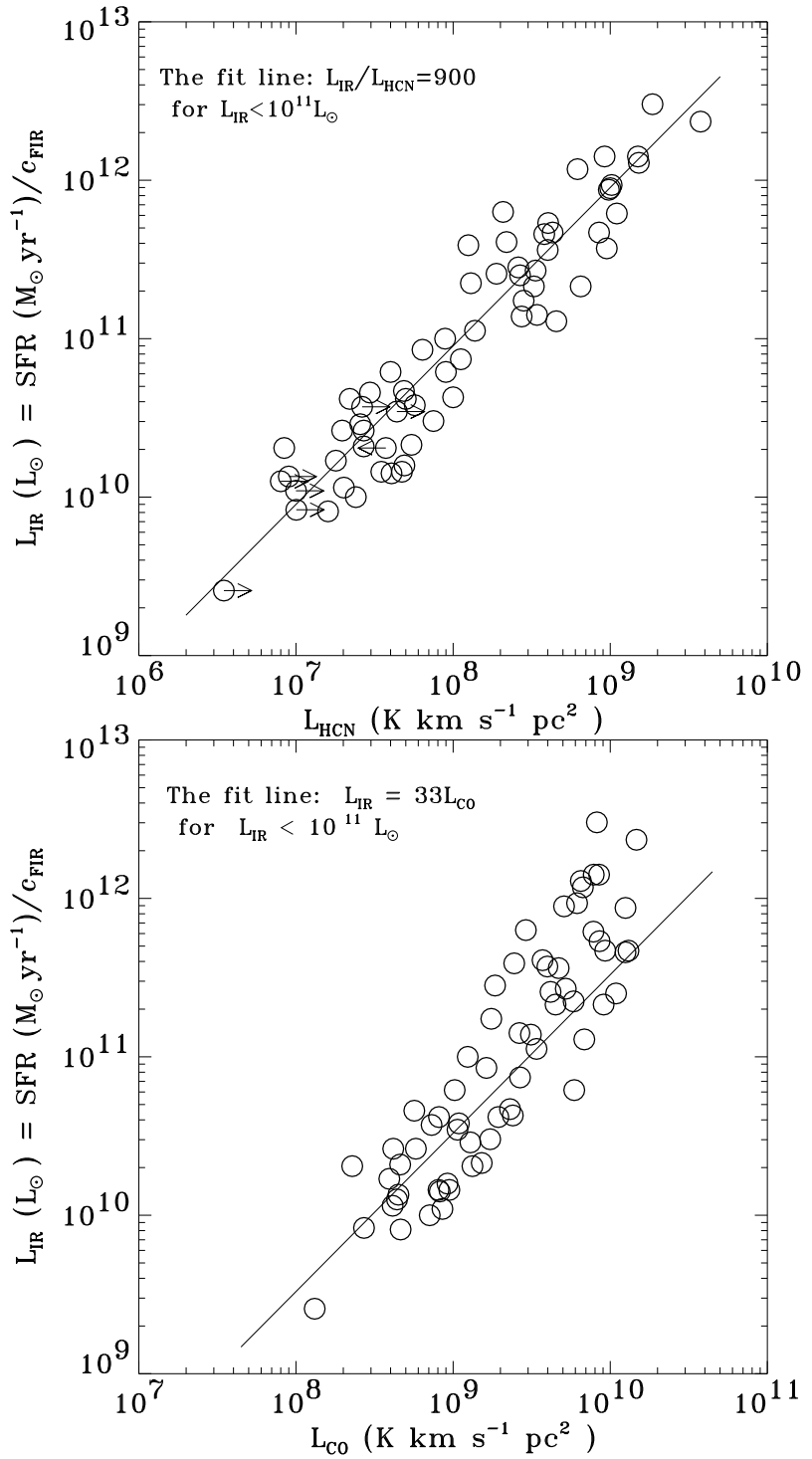


Fig. 1.— (a) The correlation between HCN and IR luminosities in 65 galaxies. Some limits in HCN luminosities are indicated with arrows. (b) The correlation between L_{CO} and L_{IR} for the same HCN sample. The sample is divided into luminous infrared galaxies (LIGs) and ultraluminous infrared galaxies (ULIGs) with $L_{\text{IR}} \geq 10^{11} L_{\odot}$ and less luminous “normal” spiral galaxies. The solid lines are the fits to the less luminous galaxies with a slope fixed at unity. A single slope of 1.0 fits HCN data for both low and high IR luminosities, but not for the CO data.

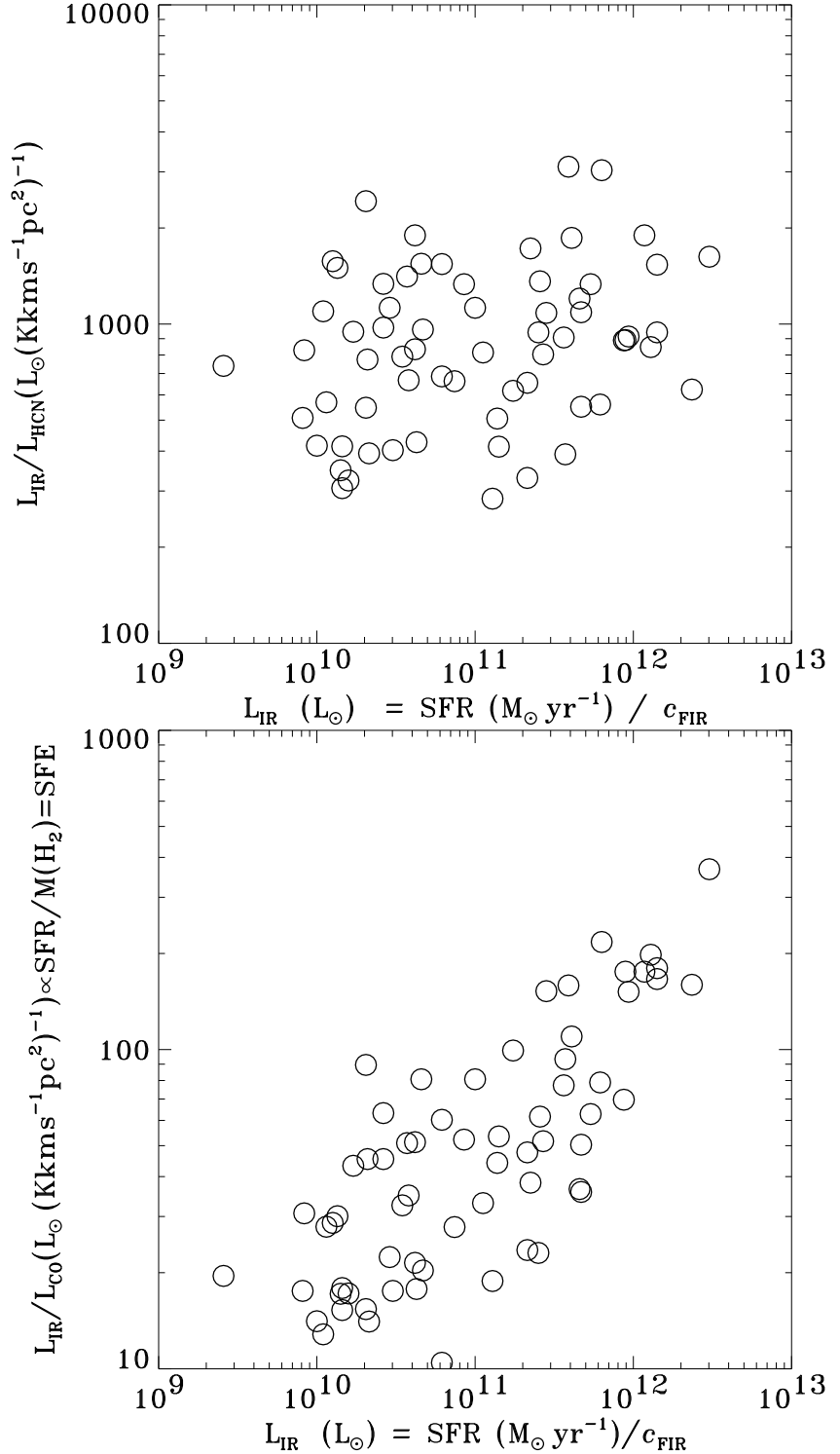


Fig. 2.— (a) The correlation between IR/HCN and IR is almost of nonexistence; (b) whereas the correlation between $L_{\text{IR}}/L_{\text{CO}}$ and L_{IR} is rather prominent. The different trends are particularly obvious at high IR luminosity for LIGs and ULIGs with $L_{\text{IR}} \geq 10^{11}L_{\odot}$.

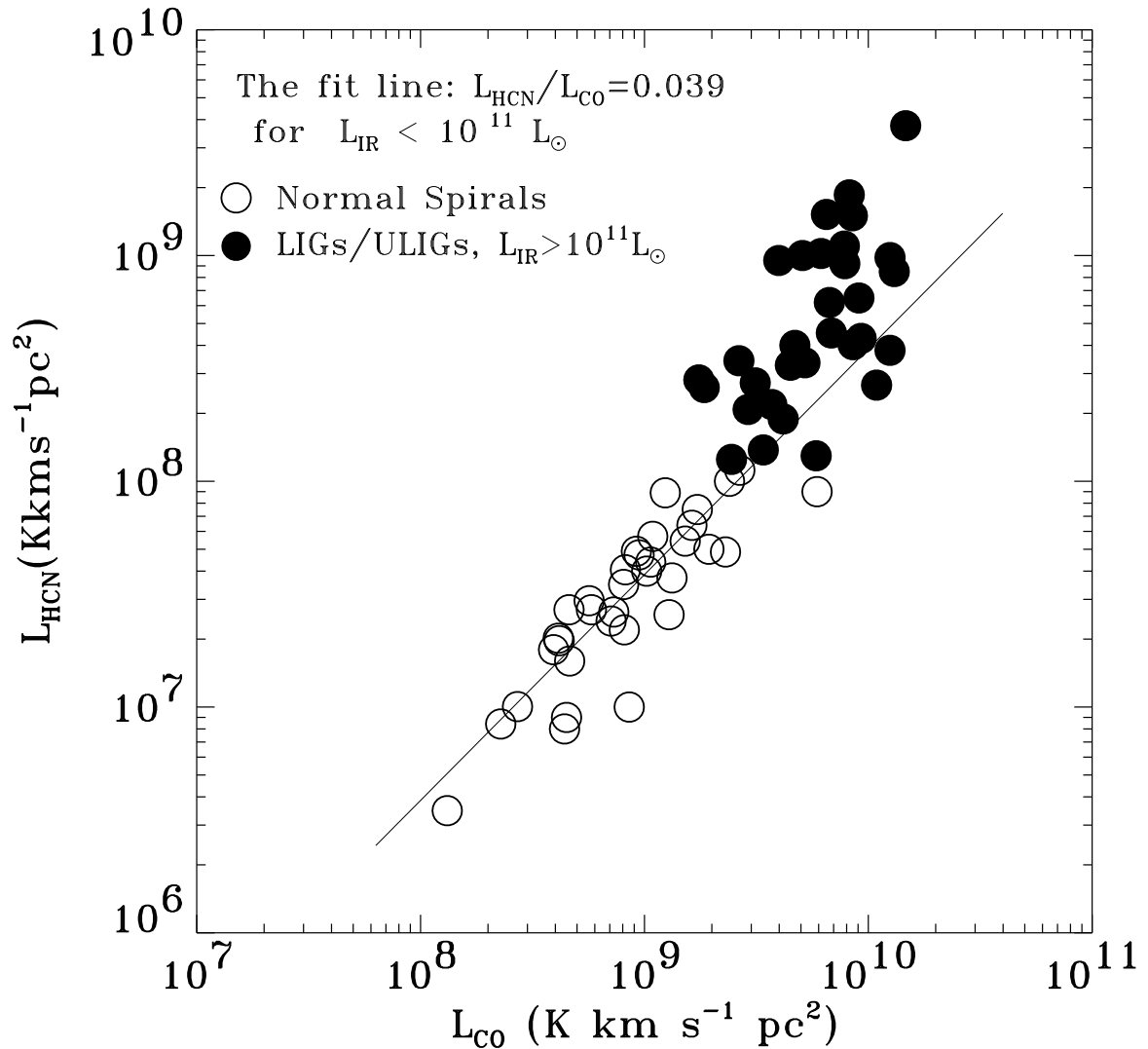


Fig. 3.— Strong correlation exists between L_{HCN} and L_{CO} indicating that the more molecular gas-rich galaxies tend to have larger amount of dense molecular gas as well. Similar to Figure 1b, the fit line is for less luminous normal galaxies (open circles) with a fixed slope at unity. Apparently, almost all LIGs and ULIGs ($L_{\text{IR}} \geq 10^{11} L_{\odot}$) lie above the line.

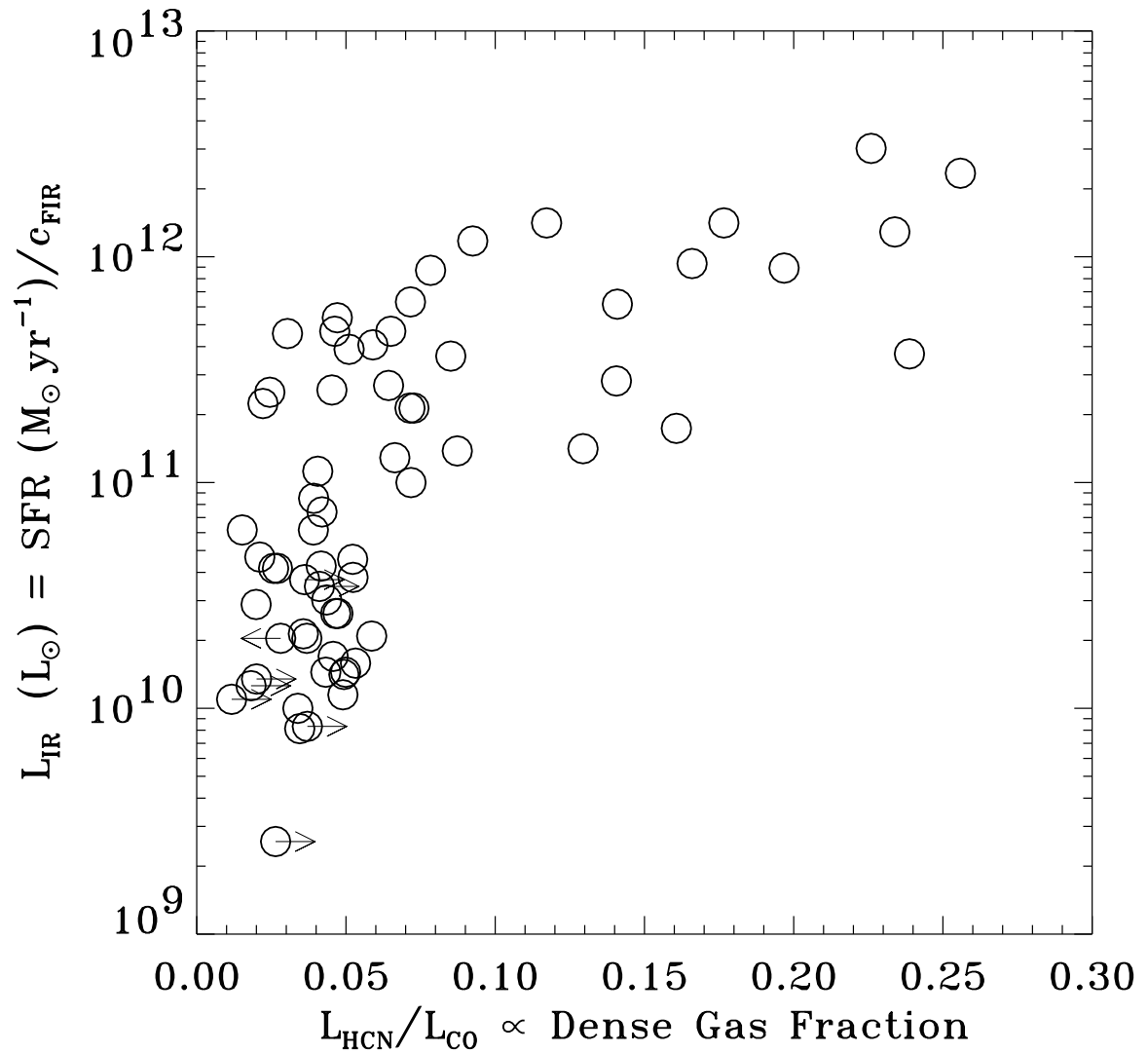


Fig. 4.— $L_{\text{HCN}}/L_{\text{CO}}$ stays at fairly small values for normal spiral galaxies, but increases dramatically for LIGs and ULIGs ($L_{\text{IR}} \geq 10^{11}L_{\odot}$). All galaxies with $L_{\text{HCN}}/L_{\text{CO}} \gtrsim 0.06$ in the sample are luminous and ultraluminous galaxies.

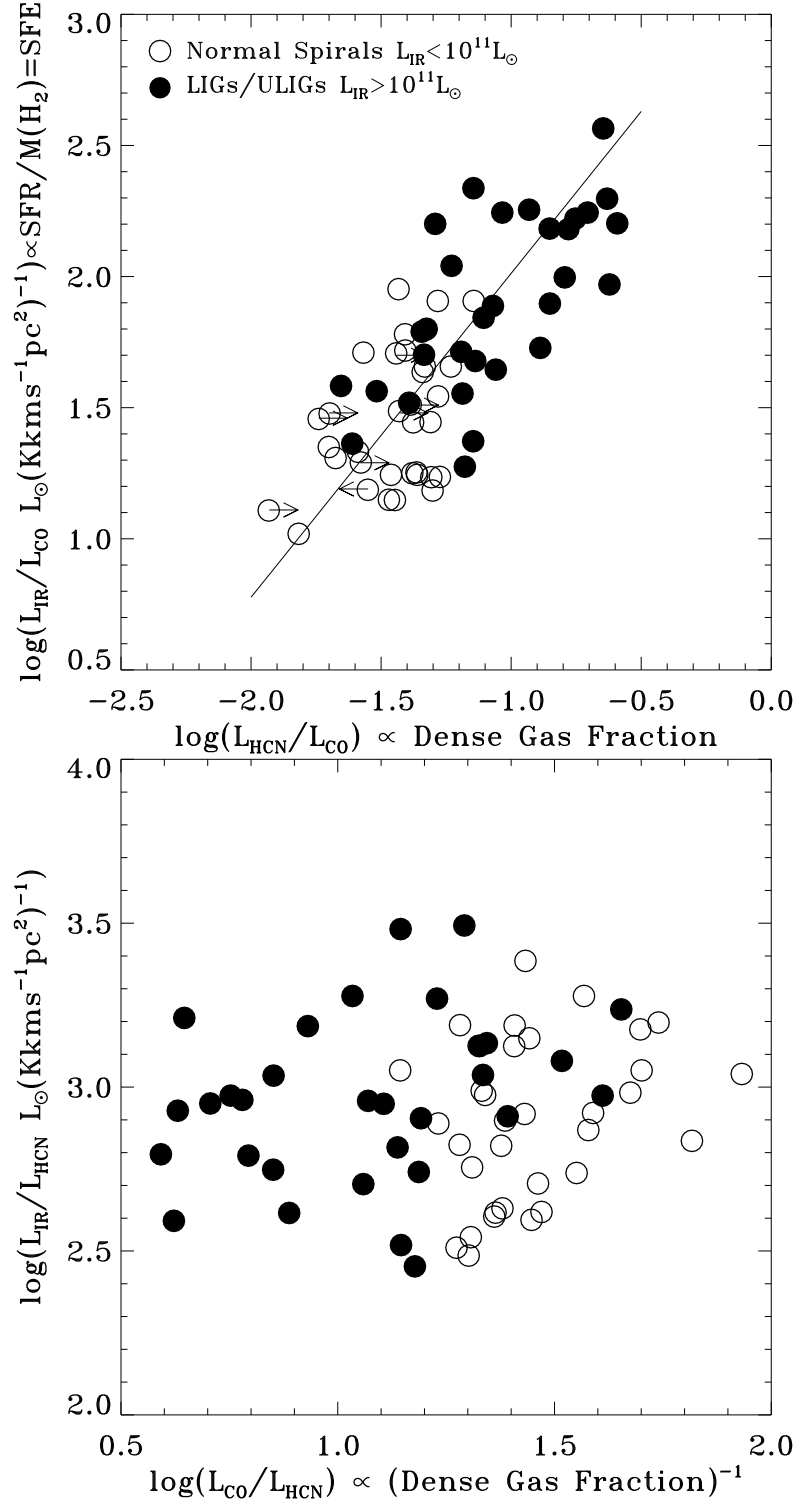


Fig. 5.— (a) Correlation between $L_{\text{HCN}}/L_{\text{CO}}$ and $L_{\text{IR}}/L_{\text{CO}}$ revealing the true relationship between the HCN and IR since both luminosities are normalized by L_{CO} . This removes all dependence on distance and galaxy size and shows that there is a true physical correlation between the IR and HCN luminosities. The best fit has a correlation coefficient of 0.74. (b) No correlation between $L_{\text{IR}}/L_{\text{HCN}}$ and $L_{\text{CO}}/L_{\text{HCN}}$ (a correlation coefficient of 0.1) suggests that the correlation between L_{IR} and L_{CO} observed in Figure 1b may not be a truly physical relation. The sample is divided into LIGs and ULIGs with $L_{\text{IR}} \geq 10^{11} L_\odot$ (filled circles) and less luminous normal spiral galaxies (open circles).

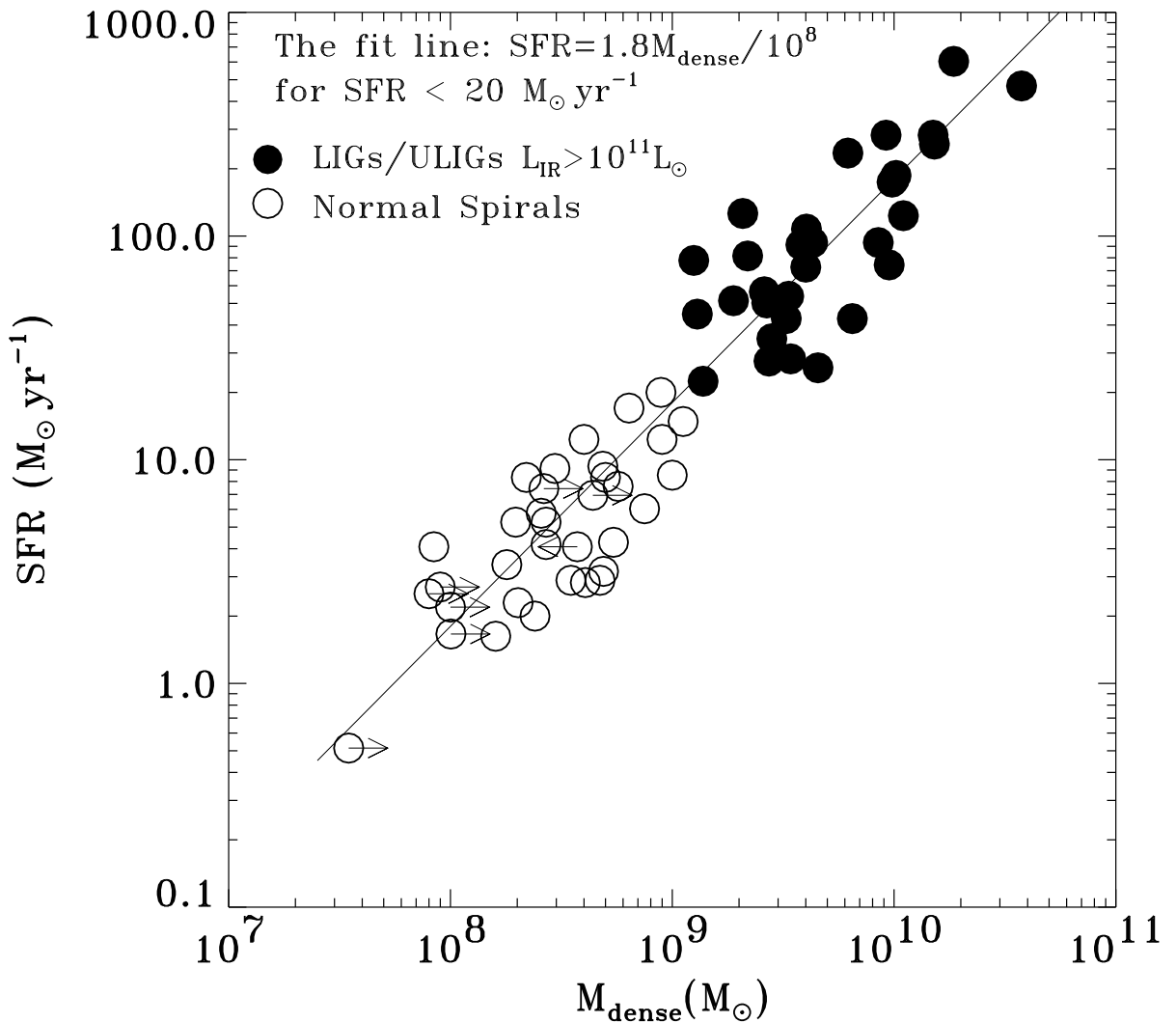


Fig. 6.— The global star formation law of dense molecular gas. The star formation rate is linearly proportional to the dense molecular gas mass. The solid circles are for LIGs and ULIGs with $L_{\text{IR}} \gtrsim 10^{11} L_{\odot}$, whereas the open circles are for the less luminous normal spiral galaxies.

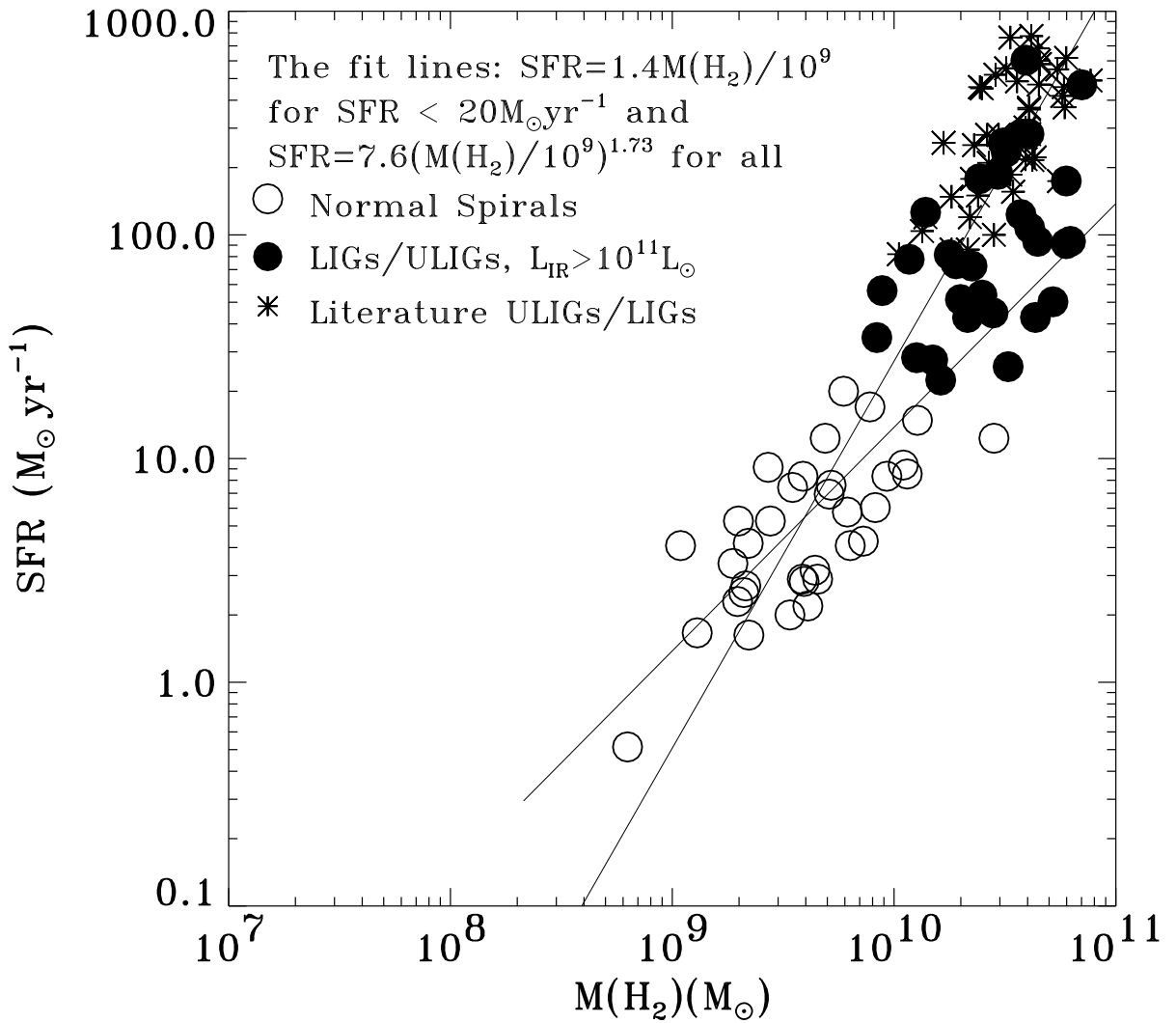


Fig. 7.— The star formation rate vs. total molecular gas mass. The solid circles are for LIGs and ULIGs with $L_{\text{IR}} \gtrsim 10^{11}L_\odot$, whereas the open circles are for the less luminous normal spiral galaxies. More CO data of mostly ULIGs available from literature (stars) are added to our HCN sample (see Fig. 1b). The orthogonal least-squares fit now has a slope of 1.73 with a correlation coefficient $R = 0.89$. The line of fixed slope of 1, a valid fit for normal spirals, is also shown for comparison.

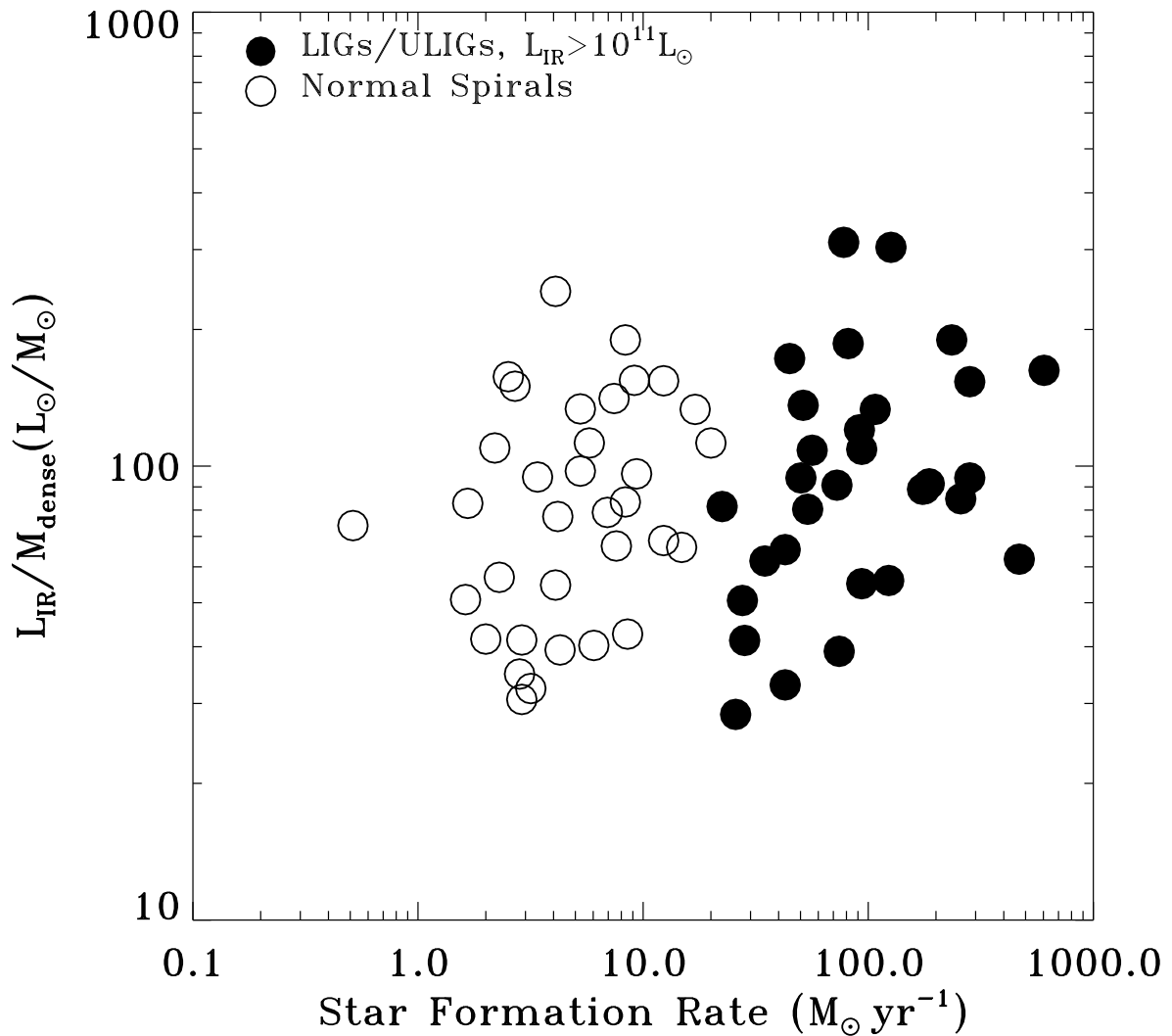


Fig. 8.— The star formation rate (far-IR luminosity) per unit of *dense* molecular gas mass is essentially independent of the total IR luminosity. The average for the entire sample is $L_{\text{IR}}/\text{M}_{\text{dense}} = 90 \text{L}_\odot/\text{M}_\odot$.

A. Correlations with the Warm Dust Temperature

The temperature T_{dust} can be estimated as a function of $f_{60\mu\text{m}}/f_{100\mu\text{m}}$ and β , where the emissivity is the Planck function of a single warm dust temperature times the frequency to the power of β , i.e., ν^β . This is for warm dust T_{dust} between ~ 25 and 60 K and $\beta \sim 1-2$ (e.g., see the appendix of Lonsdale et al. 1985). Although there is increasing evidence for a substantial amount of cold dust in spiral galaxies (e.g., Alton et al. 2000), the warm dust is probably still the most important component, especially in luminous and ultraluminous infrared galaxies (LIGs and ULIGs), and often a single dust temperature fitting of the far-IR spectral energy distribution (SED) including submillimeter measurements is still a good approximation (e.g., Lisenfeld, Isaak, & Hills 2000; Dunne et al. 2000).

The tightness of the IR–HCN correlation can be further examined by comparing the ratio of $L_{\text{IR}}/L_{\text{HCN}}$ with $f_{60\mu\text{m}}/f_{100\mu\text{m}}$. Figure 9a shows that $L_{\text{IR}}/L_{\text{HCN}}$ has only a weak dependence upon $f_{60\mu\text{m}}/f_{100\mu\text{m}}$ or T_{dust} , whereas Figure 9b indicates that $L_{\text{IR}}/L_{\text{CO}}$ correlates strongly with $f_{60\mu\text{m}}/f_{100\mu\text{m}}$ ($R^2 = 0.72$) or T_{dust} . The fits in terms of dust temperature have been given in equations (6) and (7). Unlike Figure 5b, where $L_{\text{IR}}/L_{\text{HCN}}$ appears to be totally independent of $L_{\text{CO}}/L_{\text{HCN}}$, Figure 9a indicates that $L_{\text{IR}}/L_{\text{HCN}}$ might still be weakly dependent upon T_{dust} . There is also a meaningful correlation between $L_{\text{HCN}}/L_{\text{CO}}$ and $f_{60\mu\text{m}}/f_{100\mu\text{m}}$ ($R^2 = 0.46$). An orthogonal fit can be obtained as $L_{\text{HCN}}/L_{\text{CO}} = 10^{-0.71} \times (f_{60\mu\text{m}}/f_{100\mu\text{m}})^{2.0 \pm 0.8}$ with a fairly large uncertainty in the slope since the correlation is not tight.

It is not surprising that $L_{\text{IR}}/L_{\text{CO}}$ is a strong function of T_{dust} since the dust radiates thermally as T_{dust}^4 to T_{dust}^6 , depending on the dust emissivity to produce IR emission (e.g., Soifer et al. 1989). Thus, Figure 9 is not independent of Figure 2 as T_{dust} is closely related to L_{IR} . And L_{CO} depends only linearly on the temperature, $\sim T_{\text{dust}}^1$, if the dust and gas are coupled and the gas is thermalized with the intrinsic brightness temperature $T_b \sim T_{\text{dust}}^1$ (e.g., the black-body model of Solomon et al. 1997), and more weakly in the power of T_{dust} dependence if not coupled/thermalized. HCN luminosity seems also to depend, at a first glance, only on the first power of T_{dust} if $T_b \sim T_{\text{dust}}^1$, but it is actually not simply proportional to T_{dust}^1 since the HCN emission does not fill the source area probed by the telescope beam, whereas CO has probably an area filling factor close to unity, especially for LIGs/ULIGs. Recent interferometric HCN imaging in some nearby galaxies indeed shows much smaller HCN source size than that of CO (e.g., Downes et al. 1992; Helfer & Blitz 1997a; Kohno et al. 1996, 1999). It is possible that the HCN filling factor depends on some power of T_{dust} . In addition, the weak correlation between $L_{\text{IR}}/L_{\text{HCN}}$ and T_{dust} indicates that there might be other important parameters, probably the molecular gas density, responsible for the high L_{HCN} in LIGs/ULIGs. Thus, L_{HCN} depends on a much higher power of T_{dust} , and the ratio of $L_{\text{HCN}}/L_{\text{CO}}$ should depend fairly strongly on some power of T_{dust} (eq. [8]) rather than being independent.

This rather strong T_{dust} dependence of L_{HCN} can be understood since $L_{\text{HCN}}/L_{\text{CO}}$ also correlates with L_{IR} (Fig. 4). Because the $L_{\text{HCN}}/L_{\text{CO}}$ ratio is such a good indicator of starburst and most LIGs/ULIGs have the highest $L_{\text{HCN}}/L_{\text{CO}}$ ratio, warmer LIGs/ULIGs of higher T_{dust} (higher L_{IR}) should have a higher fraction of the dense molecular gas (higher $L_{\text{HCN}}/L_{\text{CO}}$), and thus very likely high average gas density. Therefore, L_{IR} somehow correlates with the molecular gas density and T_{dust} is thus also related to the gas density, which should be expected as the gas and dust are somehow coupled.

B. Other Correlations and Model Fits

B.1. Simple Two-parameter Fits

Although L_{HCN} and L_{CO} are strongly correlated (Fig. 3), there are significant differences, however, when they are compared with either $L_{100\mu\text{m}}$ or L_{IR} (Table B1). The better correlation between L_{HCN} and L_{IR} (vs L_{CO} and L_{IR}) can be recognized in both R^2 (§3.1) and the R.M.S. deviations of the correlation fits (Table 3, 0.24 vs 0.34). The luminosity $L_{100\mu\text{m}}$ also correlates better with L_{HCN} than with L_{CO} as the difference in R^2 is also significant (0.89 vs 0.80). Nevertheless, L_{CO} appears to be much better correlated with $L_{100\mu\text{m}}$ than with L_{IR} (there is a significant difference in the logarithmic R.M.S. deviations: 0.22 vs 0.34), though the difference in R^2 (0.80 vs 0.77) is small. In comparison, there is little difference in the correlations between $L_{100\mu\text{m}}$ and L_{HCN} vs between L_{IR} and L_{HCN} ($R^2=0.89$ vs 0.87 and logarithmic R.M.S. 0.22 vs 0.23). But the HCN correlations are much tighter than the CO correlations, even though the $L_{100\mu\text{m}}-L_{\text{CO}}$ correlation has same R.M.S. deviation.

The luminosity $L_{100\mu\text{m}}$ traces relatively the cooler component of the warm dust emission at $T_{\text{dust}} \sim 25\text{--}50$ K. In this regime the 100 μm emission is a reasonable tracer of the warm dust mass M_{dust} . In comparison, the total IR luminosity L_{IR} contains the mixture of the various dust components including the hot dust radiated at the mid-IR emission. We here estimate the warm dust mass M_{dust} from the 100 μm flux density and the warm dust temperature T_{dust} and correlate it with L_{HCN} and L_{CO} in Table 3 as well. It appears that L_{CO} is only slightly better correlated with M_{dust} than L_{HCN} with M_{dust} . In short, the differences in the above-mentioned various correlations suggest that HCN is a much better tracer of both the total IR and 100 μm emission than CO, whereas CO only traces better the 100 μm than the total IR emission. The dense molecular gas rather than the total molecular gas is more intimately related to both the total IR and 100 μm emission.

B.2. Multi-parameter Fits

The predicted L_{IR} from the CO and T_{dust} [the $\text{IR}(L_{\text{CO}}, T_{\text{dust}})$ model, $\log L_{\text{IR}}(L_{\text{CO}}, T_{\text{dust}}, \text{model_fit}) = -6.34 + 0.97 \log L_{\text{CO}} + 5.4 \log T_{\text{dust}}$] turns out to be the tightest correlation ($R^2 = 0.94$) among all. The prediction of L_{IR} from CO and T_{dust} is more accurate than from HCN alone and also slightly better than from HCN plus T_{dust} . This surely suggests the importance of T_{dust} when the total molecular gas content, rather than the dense molecular gas, is concerned in predicting L_{IR} . This also implies that T_{dust} is an important parameter in regulating star formation of the total molecular gas, but not necessarily the dense (active star-forming) molecular gas.

We also use T_{dust} as well as $L_{100\mu\text{m}}$ and $L_{60\mu\text{m}}$, though they are not independent, in the three-parameter model fits as listed in Table 3, and we find the following:

1. The value of L_{CO} decreases with T_{dust} for given $L_{100\mu\text{m}}$ or L_{IR} . The value of L_{HCN} is, however, linearly proportional to $L_{100\mu\text{m}}$ or L_{IR} with no correction or only marginal correction of T_{dust} . Thus, L_{HCN} decreases little with T_{dust} for a given $L_{100\mu\text{m}}$ or L_{IR} . To put it in a different perspective, L_{IR} is only slightly better predicted when T_{dust} is considered together with L_{HCN} , whereas L_{IR} is much better predicted when both L_{CO} and T_{dust} are in the fit.
2. The $\text{HCN}(L_{\text{CO}}, T_{\text{dust}})$ model implies that HCN correlates with T_{dust} to the 3.3 power as well as linearly (the first power) with L_{CO} (cf. Equation 8). Thus, HCN responds sensitively to T_{dust} with a

Table 3. Model Fit Parameters

Para.	$L_{60\mu\text{m}}$	$L_{100\mu\text{m}}$	L_{IR}	T_{dust}	L_{HCN}	L_{CO}	Const.	RMS ^a	R^2 ^b
3 parameter correlations									
L_{IR}					0.88	0.16	2.29	0.24	0.87
L_{IR}			5.4		0.97	−6.34	0.17	0.17	0.94
L_{IR}			2.9	0.86		−0.48	0.20	0.20	0.92
L_{HCN}			3.3		1.00	−6.22	0.21	0.21	0.89
L_{HCN}		0.56			0.49	−2.62	0.19	0.19	0.90
L_{HCN}		0.96	(−1.7)			0.17	0.21	0.21	0.89
L_{CO}		0.89	−4.4			6.27	0.17	0.17	0.88
L_{HCN}	0.95		(−0.2)			−1.12	0.21	0.21	0.89
L_{CO}	0.88		−3.0			5.07	0.17	0.17	0.88
L_{HCN}	(−.06)	1.01				−1.41	0.21	0.21	0.89
L_{CO}	−1.13	2.02				0.47	0.17	0.17	0.88
simple 2 parameter correlations									
L_{IR}					1.25	0.72	0.34	0.77	
L_{IR}				1.02		2.58	0.24	0.24	0.88
L_{HCN}					1.26	−3.73	0.28	0.28	0.85
L_{HCN}		0.91				−1.93	0.23	0.23	0.87
L_{HCN}	0.96					−1.52	0.22	0.22	0.89
L_{CO}	0.72					−2.12	0.22	0.22	0.80
L_{CO}		0.62				2.49	0.30	0.30	0.75
L_{CO}				0.67		3.92	0.27	0.27	0.85
M_{dust}					0.84	0.41	0.25	0.25	0.84
M_{dust}						1.13	−3.35	0.21	0.87

^arms = Root Mean Square deviation (logarithmic) between the data (observed) and the predicted from the (correlation) model fits.

^bThe squared correlation coefficient R^2 .

Note. — All quantities are logarithmic in the correlation fits. The line luminosities are in units of $\text{Kkm s}^{-1}\text{pc}^2$ and the total IR, 60, and 100 μm luminosities are in units of L_\odot , while T_{dust} is in K. The warm dust mass M_{dust} was estimated using only the 100 μm flux and warm dust temperature. The model fit for L_{IR} from L_{HCN} and L_{CO} (the IR(L_{HCN} , L_{CO}) model), for example, is $\log L_{\text{IR}}(\text{predicted}) = 0.88\log L_{\text{HCN}} + 0.16\log L_{\text{CO}} + 2.3$ with the correlation coefficient $R = 0.93$ ($R^2 = 0.87$) and the rms error is $(\sum[\log L_{\text{IR}}(\text{predicted}) - \log L_{\text{IR}}(\text{obs.})]^2/N)^{1/2} = 0.24$. Numbers with parentheses indicate only marginal significance.

power of $\gtrsim 4.3$. The $\text{IR}(L_{\text{HCN}}, T_{\text{dust}})$ model gives a 2.9 power correlation with T_{dust} and a 0.86 power with L_{HCN} , again roughly consistent with the high (~ 6) power T_{dust} dependence (cf. eq. [6]) when the T_{dust} dependence of L_{HCN} (eq. [8]) has been considered. In short, the difference in the dependences of the HCN and IR upon the warm dust temperature is not dramatic. Thus, the ratio of $L_{\text{IR}}/L_{\text{HCN}}$ has only a weak dependence upon T_{dust} (eq. [7] and Fig. 9a).

3. The $\text{HCN}(L_{60\mu\text{m}}, L_{100\mu\text{m}})$ model fit and $\text{CO}(L_{60\mu\text{m}}, L_{100\mu\text{m}})$ 3 parameter correlation model reveal that HCN correlates primarily with $L_{100\mu\text{m}}$, and essentially not at all with $L_{60\mu\text{m}}$, whereas CO correlates with both $L_{60\mu\text{m}}$ and $L_{100\mu\text{m}}$. This again implies the much tighter dependence of CO upon T_{dust} , and is basically reiterating the first point described above since there are only two independent parameters among T_{dust} , $L_{60\mu\text{m}}$, $L_{100\mu\text{m}}$ and L_{IR} .

B.3. Fits Between the Ratios

Figures 4 and 5 already showed some correlations between the parameter ratios. Here we just list the weak correlation between $L_{\text{IR}}/L_{\text{HCN}}$ and $f_{60\mu\text{m}}/f_{100\mu\text{m}}$ ($R^2=0.17$, Fig. 9a), as directly obtained from the orthogonal fit, $L_{\text{IR}}/L_{\text{HCN}} = 10^{3.1} \times (f_{60\mu\text{m}}/f_{100\mu\text{m}})^{0.63}$ with a logarithmic R.M.S. of 0.21. The T_{dust} power and the fit have large scatters owing to the poor correlation. The scatter is about the same or only slightly better than the R.M.S. of the observed mean luminosity ratio (in logarithm) of $\log \langle L_{\text{IR}}/L_{\text{HCN}} \rangle$ for the entire sample, which is ~ 0.23 . The correlation fit for $L_{\text{IR}}/L_{\text{CO}}$ vs $f_{60\mu\text{m}}/f_{100\mu\text{m}}$ or T_{dust} (Fig. 9b, eq. [6]) is significantly tighter and has a logarithmic R.M.S. of 0.17. This small R.M.S. is obviously much better than the R.M.S. of the observed mean $\log \langle L_{\text{IR}}/L_{\text{CO}} \rangle$ of the entire sample, which is ~ 0.37 .

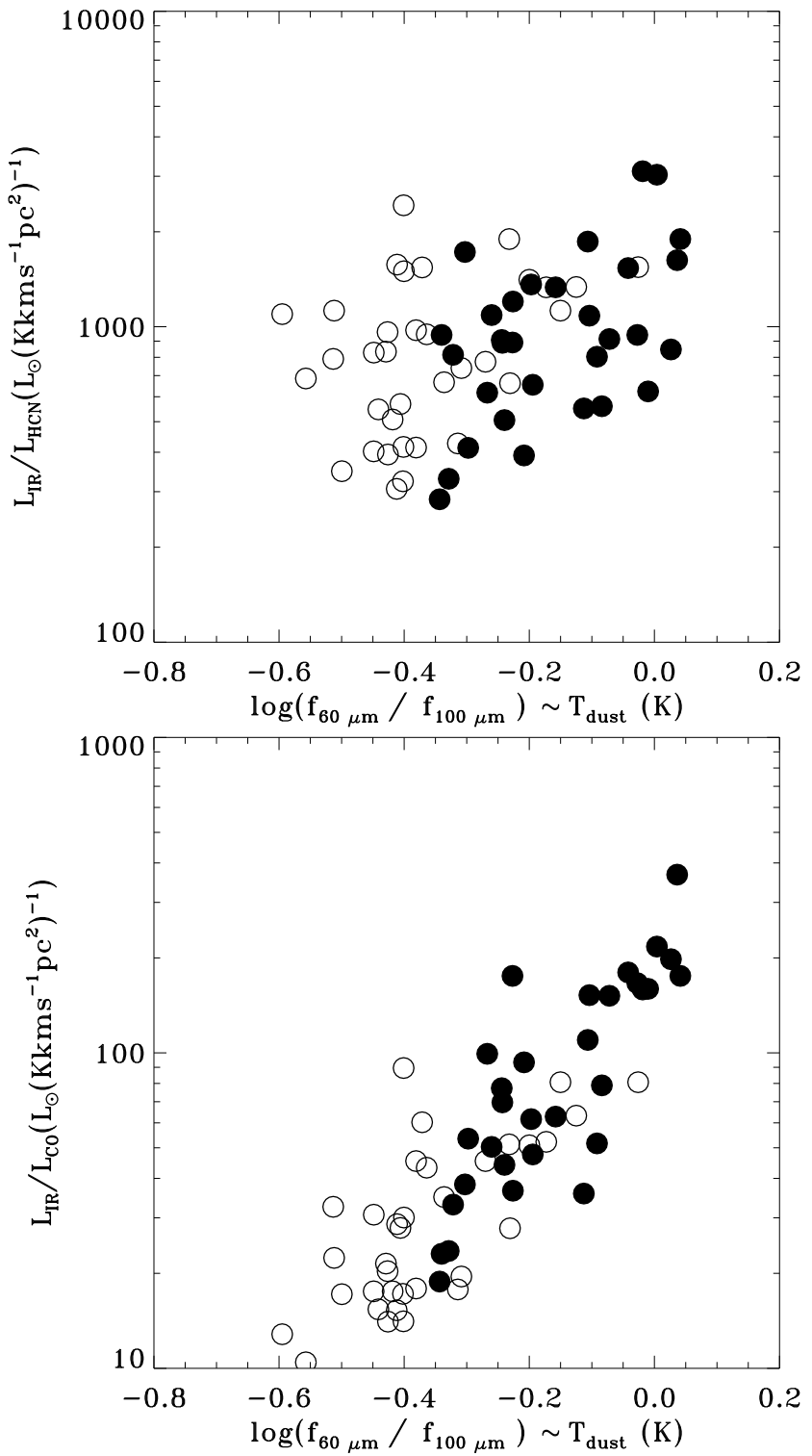


Fig. 9.— (a) $L_{\text{IR}}/L_{\text{HCN}}$ as a function of the far-infrared (FIR) color (the $60\mu\text{m}$ -to- $100\mu\text{m}$ flux ratio) which indicates the warm dust temperature T_{dust} . (b) $L_{\text{IR}}/L_{\text{CO}}$ as a function of the FIR color (or T_{dust}). There is only weak correlation between $L_{\text{IR}}/L_{\text{HCN}}$ and T_{dust} , whereas strong correlation exists between $L_{\text{IR}}/L_{\text{CO}}$ and T_{dust} . For optically thin dust with emissivity $\propto \nu^{1.5}$, T_{dust} is approximately in a range of 25–50 K for galaxies in our sample. The sample is divided into luminous and ultraluminous infrared galaxies (LIGs/ULIGs) with $L_{\text{IR}} \geq 10^{11} \text{L}_\odot$ (filled circles) and less luminous galaxies (open circles).

REFERENCES

Aalto, S., Booth, R.S., Black, J.H. & Johansson, L.E.B. 1995, A&A, 300, 369

Aalto, S., Radford, S.J.E., Scoville, N.Z., & Sargent, A.I. 1997, ApJ, 475, L107

Alton, P.B., Trewella, M., Davies, J.I., Evans, R., Bianchi, S., Gear, W., Thronson, H., Valentijn, E., Witt, A. 1998a, A&A, 335, 807

Alton, P.B., Bianchi, S., Rand, R.J., Xilouris, E. M., Davies, J.I., & Trewella, M. 1998b, ApJ, 507, L125

Alton, P.B., Xilouris, E.M., Bianchi, S., Davies, J., & Kylafis, N. 2000, A&A, 356, 795

Bloeman, J.B.G.M., et al. 1986 A&A, 154, 25

Bryant, P.M., & Scoville, N.Z. 1999, AJ, 117, 2632

Carilli, C.L., Cox, P., Bertoldi, F. et al. 2002, ApJ, 575, 145

Casoli, F., Dupraz, C., & Combes, F. 1992, A&A, 264, 49

Casoli, F., Willaime, M.-C., Viallefond, F., & Gerin, M. 1999, A&A, 346, 663

Chapman, S.C., Blain, A.W., Ivison, R.J., & Smail, I. 2003, Nature, 422, 695

Condon, J.J., Huang, Z.-P., Yin, Q.F., & Thuan, T.X. 1991, ApJ, 378, 65

Cox, P. Omont, A., Djorgovski, S.G. et al. 2002, A&A, 387, 406 (astro-ph/0203355)

Curran, S.J., Aalto, S., & Booth, R.S. 2000, A&AS, 141, 193

Curran, S.J., Polatidis, A. G., Aalto, S., & Booth, R.S. 2001, A&A, 368, 824

Davies, J.I., Alton, P., Trewella, M., Evans, R., & Bianchi, S. 1999, MNRAS, 304, 495

Devereux, N.A., & Young, J.S. 1990, ApJ, 350, L25

Devereux, N.A., & Young, J.S. 1992, AJ, 103, 1536

Devereux, N.A., & Young, J.S. 1993, AJ, 106, 948

Downes, D., Radford, S.J.E., Guilloteau, S., et al. 1992, A&A, 262, 424

Downes, D., & Solomon, P.M. 1998, ApJ, 507, 615

Downes, D., Neri, R., Wiklind, T., Wilner, D.J., & Shaver, P.A. 1999, ApJ, 513, L1

Dunne, L., Eales, S., Edmunds, M., Ivison, R., Alexander, P., & Clements, D.L. 2000, MNRAS, 315, 115

Evans, N.J., II 1999, ARA&A, 37, 311

Franceschini, A., Braito, V., Persic, M. et al. 2003, MNRAS, 343, 1181

Frayer, D.T. et al. 1998, ApJ, 506, L7

Gao, Y. 1996, Ph.D. thesis, SUNY at Stony Brook

Gao, Y. 1997, PASP, 109, 1189

Gao, Y., Solomon, P.M., Downes, D., & Radford, S.J.E. 1997, ApJ, 481, L35

Gao, Y., & Solomon, P.M. 1999, ApJ, 512, L99

Gao, Y., Gruendl, R.A., Hwang, C.-Y., & Lo, K.Y. 1999, in IAU 186, 227

Gao, Y., & Solomon, P.M. 2003, ApJ, submitted (Paper I)

Gallagher, J.S., & Hunter, D.A. 1987, in *Star Formation in Galaxies*, ed. C. Lonsdale, (Washington: Gov't Ptg Office), p. 167

Gehrz, R.D., Sramek, R.A., & Weedman, D.W. 1983, 267, 551

Genzel, R., et al 1998, ApJ, 498, 579

Greve, T.R., Ivison, R.J., & Papadopoulos, P.P. 2003, ApJ, 599, 839 (astro-ph/0309213)

Guilloteau, S. et al. 1999, A&A, 349, 363

Haas, M., Lemke, D., Stickel, M. et al. 1998, A&A, 338, 33

Heckman, T.M. 2000, Philos.Trans.R.Soc.London, A, 358, 2077

Helfer, T.T., & Blitz, L. 1993, ApJ, 419, 86

Helfer, T.T., & Blitz, L. 1995, ApJ, 450, 90

Helfer, T.T., & Blitz, L. 1997a, ApJ, 478, 162

Helfer, T.T., & Blitz, L. 1997b, ApJ, 478, 233

Henkel, C., Whiteoak, J.B., Nyman, L.-Å., & Harju, J. 1990, A&A, 230, L5

Henkel, C., Whiteoak, J.B., & Mauersberger, R. 1994, A&A, 284, 17

Hwang, C.-Y., Lo, K.Y., Gao, Y., Gruendl, R.A., & Lu, N.Y. 1999, ApJ, 511, L17

Isaak, K.G., et al. 2002, MNRAS, 329, 149

Israel, F.P. 1992, A&A, 265, 487

Jackson, J.M., Paglione, T.A.D., Ishizuki, S., & Nguyen-Q-Rieu 1993, ApJ, 418, L13

Jackson, J.M., Heyer, M.H., Paglione, T.A.D., & Bolatto, A.D. 1996, ApJ, 456, L91

Joseph, R. 1999, Ap&SS, 266, 321

Kennicutt, R.C. 1998a, ApJ, 498, 541

Kennicutt, R.C. 1998b, ARA&A, 36, 189

Kohno, K., et al. 2003, PASJ, 55, L1

Kohno, K., Kawabe, R., & Vila-Vilaro, B. 1999, ApJ, 511, 157

Kohno, K., Kawabe, R., Tosaki, T., & Okumura, S.K. 1996, ApJ, 461, L29

Lee, Y., Snell, R.L., & Dickman, R.L. 1990, ApJ, 355, 536

Lisenfeld, U., Isaak, K.G., & Hills, R. 2000, MNRAS, 312, 433

Lo, K.Y., Gao, Y., & Gruendl, R.A. 1997, 475, L103

Lonsdale, C.J., Helou, G., Good, J.C., & Rice, W. 1985, *Cataloged galaxies and quasars observed in the IRAS survey* (Pasadena: JPL)

Luhman, M.L., Satyapal, S., Fischer, J., Wolfire, M.G., Sturm, E., Dudley, C.C., Lutz, D., & Genzel, R. 2003, ApJ, 594, 758

Mauersberger, R., & Henkel, C. 1993, Rev. Modern Astron., 6, 69

Meier, D.S., & Turner, J.L. 2001, ApJ, 551, 687

Mirabel, I.F., et al. 1990, A&A, 236, 327

Mooney, T.J., & Solomon, P.M. 1988, ApJ, 334, L51

Nagar, N.M., ilson, A.S., Falcke, H., Veilleux, S., & Maiolino, R. 2003, A&A, 409, 115 (astro-ph/0309298)

Neri, R., et al. 2003, ApJ, in press (astro-ph/0307310)

Nguyen-Q-Rieu, Nakai, N. & Jackson, J.M. 1989, A&A, 220, 57

Nguyen-Q-Rieu, Jackson, J.M., Henkel, C., Truon-Bach & Mauersberger, R. 1992, ApJ, 399, 521

Omont, A., et al. 2001, A&A, 374, 371

Paglione, T.A.D., Tosaki, T., & Jackson, J.M. 1995, ApJ, 454, L117

Paglione, T.A.D., Jackson, J.M., & Ishizuki, S. 1997, ApJ, 484, 656

Papadopoulos, P.P., Ivison, R., Carilli, C., & Lewis, G. 2001, Nature, 409, 58

Pirogov, L. 1999, A&A, 348, 600

Plume, R., Jaffe, D.T., Evans, N.J. II, et al. 1997, ApJ, 476, 730

Popescu, C.C., Tuffs, R.J., Kylafis, N.D., Madore, B.F. 2004, A&A, 414, 45

Radford, S.J.E., Delannoy, J., Downes, D., et al. 1991, in IAU Symp 146, *Dynamics of Galaxies and their Molecular Cloud Distributions*, ed. F. Combes, & F. Casoli (Dordrecht: Kluwer), 303

Radford, S.J.E. 1994, in *The Cold Universe*, ed. T. Montmerle, C.J. Lada, I.F. Mirabel, J. Tran Thanh Van, (Gif-sun-Yvette: Ed Frontieres) p. 369

Reynaud, D. & Downes, D. 1997, A&A, 319, 737

Rice, W. 1993, AJ, 105, 67

Rice, W., et al. 1988, ApJS, 68, 91

Rowan-Robinson, M. 2000, MNRAS, 316, 885

Rownd, B.K., & Young, J.S. 1999, AJ, 118, 670

Sakamoto, K., et al. 1999, ApJ, 514, 68

Sanders, D.B., Soifer, B.T., Elias, J.H., Madore, B.F., Matthews, K., Neugebauer, G., & Scoville, N.Z. 1988, ApJ, 325, 74

Sanders, D.B., Phinney, E.S., Neugebauer, G., Soifer, B.T., & Matthews, K. 1989, ApJ, 347, 29

Sanders, D.B., Scoville, N.Z., & Soifer, B.T. 1991, ApJ, 370, 158

Sanders, D.B., & Mirabel, I.F. 1996, ARA&A, 34, 749

Sanders, D.B. 1999, astro-ph/9908297

Schmidt, M. 1959, ApJ, 129, 243

Scoville, N.Z., & Young, J.S. 1983, ApJ, 265, 148

Scoville, N.Z., Yun, M.S., & Bryant, P.M. 1997, ApJ, 484, 702

Scoville, N.Z., Evans, A.S., Thompson, R. et al. 2000, AJ, 119, 991

Shibatsuka, T., Matsushita, S., Kohno, K., & Kawabe, R. 2003, PASJ, 55, 87

Soifer, B.T. et al. 1989, AJ, 98, 766

Soifer, B.T., Neugebauer, G., Matthews, K. et al. 2001, AJ, 122, 1213

Solomon, P.M., Sanders, D.B., & Scoville, N.Z. 1979, in *The Large Scale Characteristics of the Galaxy*, IAUS 84, (Dordrecht D Reidel) 35

Solomon, P.M., Rivolo, A.R., Barrett, J., & Yahil, A. 1987, ApJ, 319, 730

Solomon, P.M., & Barrett, J.W. 1991, in IAU Symp 146, *Dynamics of Galaxies and their Molecular Cloud Distributions*, ed. F. Combes, & F. Casoli (Dordrecht: Kluwer), 235

Solomon, P.M., Downes, D., & Radford, S.J.E. 1992, *ApJ*, 387, L55
Solomon, P.M., Radford, S.J.E., & Downes, D. 1990, *ApJ*, 348, L53
Solomon, P.M., Downes, D., Radford, S.J.E., & Barrett, J.W. 1997, *ApJ*, 478, 144
Solomon, P.M., & Sage, L.J. 1988, *ApJ*, 334, 613
Solomon, P.M., Vanden Bout, P., Carilli, C., & Guelin, M. 2003, *Nature*, 426, 636
Sorai, K., Nakai, N., Kuno, N., & Nishiyama, K. 2002, *PASJ*, 54, 179
Stutzki, J., Genzel, R., Harris, A.I., Herman, J., & Jaffe, D.T. 1988, 330, L125
Surace, J.A., & Sanders, D.B. 1999, *ApJ*, 512, 162
Surace, J.A., Sanders, D.B., Vacca, W.D., Veilleux, S., & Mazzarella, J.M. 1998, *ApJ*, 492, 116
Telesco, C.M., Dressel, L.L., & Wolstencroft, R.D. 1993, *ApJ*, 414, 120
Tacconi, L.J., Genzel, R., Blietz, M., Cameron, M., Harris, A. & Madden, S. 1994, *ApJ*, 426, L77
Tacconi, L.J., et al. 1997, *ApSS*, 248, 59
Turner, J.L., & Hurt, R.L. 1992, *ApJ*, 384, 72
Turner, J.L., & Ho, P.T.P. 1983, *ApJ*, 268, L79
Turner, J.L., et al. 1993, *ApJ*, 413, L19
Veilleux, S., Kim, D.C., & Sanders, D.B. 2002, *ApJS*, 143, 315
Veilleux, S., Sanders, D.B., & Kim, D.C. 1999, *ApJ*, 522, 139
Wang, W.H., Lo, K.Y., Gao, Y., & Gruendl, R.A. 2001, *AJ*, 122, 140
Wong, T., & Blitz, L. 2002, *ApJ*, 569, 157
Wild, W., & Eckart, A. 2000, *A&A*, 359, 483
Xu, C., Gao, Y., Mazzarella, J., Lu, N.Y., Sulentic, J.W., & Domingue, D.L. 2000, *ApJ*, 541, 644
Young, J.S., Schloerb, F.P., Kenney, J.D.P., Lord, S.D. 1986, *ApJ*, 304, 443
Young, J.S., Xie, S., Kenney, J.D.P., Rice, W.L. 1989, *ApJS*, 70, 699
Young, J.S., & Scoville, N.Z. 1991, *ARA&A*, 29, 581
Young, J.S., 1999, *ApJ*, 514, L87